

# Towards reconstructing the Arctic atmospheric methane history over the 20th century: measurement and modeling results for the NGRIP firn

Taku Umezawa<sup>1</sup>, Satoshi Sugawara<sup>2</sup>, Kenji Kawamura<sup>3,4,5</sup>, Ikumi Oyabu<sup>3</sup>, Stephen J. Andrews<sup>1,6</sup>, Takuya Saito<sup>1</sup>, Shuji Aoki<sup>7</sup> and Takakiyo Nakazawa<sup>7</sup>

<sup>1</sup>National Institute for Environmental Studies, Tsukuba, Japan

<sup>2</sup>Miyagi University of Education, Sendai, Japan

<sup>3</sup>National Institute of Polar Research, Tokyo, Japan

<sup>4</sup>Department of Polar Science, The Graduate University of Advanced Studies (SOKENDAI), Tokyo, Japan

<sup>5</sup>Japan Agency for Marine Science and Technology, Yokosuka, Japan

<sup>6</sup>Wolfson Atmospheric Chemistry Laboratories, Department of Chemistry, University of York, York, UK

<sup>7</sup>Center for Atmospheric and Oceanic Studies, Graduate School of Science, Tohoku University, Sendai, Japan

Correspondence to: Taku Umezawa (umezawa.taku@nies.go.jp)

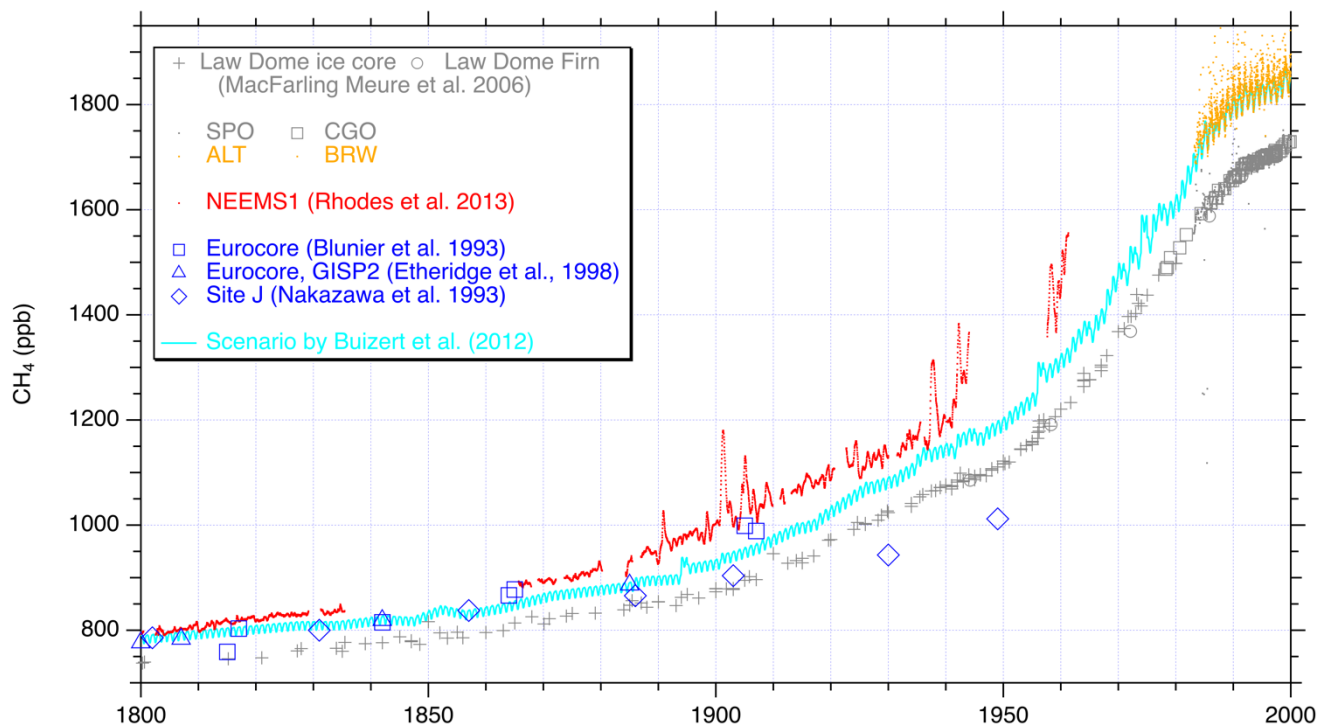
**Abstract.** Systematic measurements of atmospheric methane (CH<sub>4</sub>) mole fractions at the northern high latitudes only began in the early 1980s, and whilst CH<sub>4</sub> measurements from Greenland ice cores covered the period before ~1900, no reliable observational record is available for the intermediate period. In this study, we reconstruct the atmospheric CH<sub>4</sub> for that period, when the mole fraction started to increase rapidly. We use a data set of trace gas data measured from the air trapped in firn (an intermediate stage between snow and glacial ice formation) air samples collected at the NGRIP (North Greenland Ice Core Project) site in 2001, in combination with a firn-air transport model whose performance is validated by using a set of published firn-air data at the NEEM (North Greenland Eemian ice Drilling) site. We examine a variety of possible firn diffusivity profiles using a suite of measured trace gases, and reconstruct the CH<sub>4</sub> mole fraction by an iterative dating method based on the two Arctic firn data sets in the same manner. We find that, given the currently available firn air data sets from Greenland, reliable reconstruction of the Arctic CH<sub>4</sub> mole fraction is possible only back to before the mid 1970s. For the earlier period, is highly uncertain. Although it is difficult to accurately identify the atmospheric CH<sub>4</sub> history that consistently reproduce the depth profiles of CH<sub>4</sub> in firn at both NGRIP and NEEM sites. Therefore, the currently proposed Arctic CH<sub>4</sub> history should still be considered preliminary and uncertain, and should not be treated as the known history for constraining firn-air transport models, both firn data sets are more consistent with the atmospheric CH<sub>4</sub> scenario prepared for the NEEM firn modeling than that for the CMIP6 (Climate Model Intercomparison Project Phase 6) experiments. It is considered that the former is the current best choice for the available synthetic Arctic CH<sub>4</sub> history, but should not be treated as the known history for constraining firn-air transport models until supported by further data from sources such as Arctic ice cores. Given the current difficulty in reconstructing the CH<sub>4</sub> history from the firn-air data sets from Greenland, future sampling and measurements of ice cores at a high-accumulation site may be the only way to accurately reconstruct the atmospheric CH<sub>4</sub> trend over the 20th century.

## 1 Introduction

35 Methane (CH<sub>4</sub>) is an important atmospheric greenhouse gas emitted from both natural and anthropogenic sources. Despite  
great efforts for understanding its global budget, emission estimates of individual sources still have large quantitative  
uncertainties (e.g. Saunio et al., 2020; Chandra et al., 2021). Anthropogenic activities have enhanced CH<sub>4</sub> emissions globally  
and ~~this resulted in the~~ more than doubled the abundance of atmospheric CH<sub>4</sub> over the industrial era (e.g. Etheridge et al.,  
1998). The CH<sub>4</sub> emission histories have been estimated based on human activity statistics combined with emission factors  
40 (Stern and Kaufmann 1996; van Aardenne et al., 2001). Such historical emission inventories have been examined by  
atmospheric chemistry transport modeling (Houweling et al., 2000; Monteil et al., 2011; Ghosh et al., 2015), in combination  
with the records of atmospheric CH<sub>4</sub> mole fraction reconstructed from polar ice cores (Blunier et al., 1993; Nakazawa et al.,  
1993; Etheridge et al., 1998; MacFarling Meure et al., 2006; Sapart et al., 2012) and air extracted from porous snow layers at  
the top of ice sheets (firn) (Francey et al., 1999; Buizert et al., 2012; Sapart et al., 2013).

45 A large fraction of natural and anthropogenic CH<sub>4</sub> sources resides in the northern hemisphere, and thus the atmospheric CH<sub>4</sub>  
trend of the northern hemisphere can provide important information on the evolution of anthropogenic CH<sub>4</sub> emissions as well  
as the variations of natural CH<sub>4</sub> emission in response to climatic variability. The interhemispheric gradient of CH<sub>4</sub> mole fraction  
is also key to the allocation of CH<sub>4</sub> emissions between both hemispheres (e.g. Dlugokencky et al., 2003; Ghosh et al., 2015;  
Chandra et al., 2021).

50



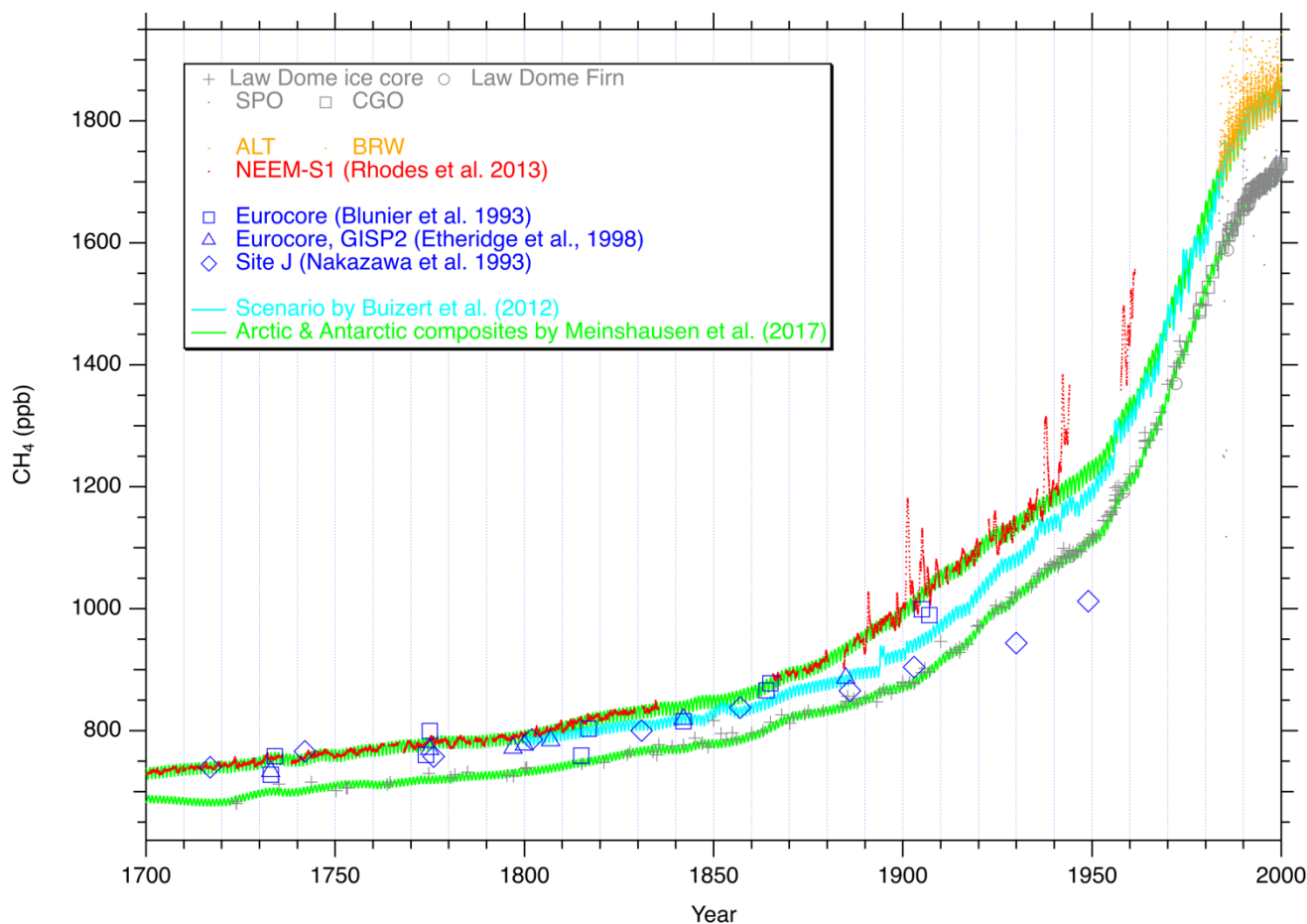


Figure 1: Atmospheric CH<sub>4</sub> mole fraction data covering the last 200 years. Symbols in grey are from the southern hemisphere; crosses and open circles are from the Law Dome ice core and firn, respectively (Etheridge et al., 1998; MacFarling Meure et al., 2006); open squares are from Cape Grim (CGO) (MacFarling Meure et al., 2006); dots are from South Pole (SPO) (<ftp://aftp.cmdl.noaa.gov/>). Colored data (except light green) from the northern hemisphere; open squares, triangles and diamonds are from the Eurocore (Blunier et al., 1993), Eurocore and GISP2 (Etheridge et al., 1998) and Site J (Nakazawa et al., 1993) ice cores; red dots are the NEEM-S1 ice core (Rhodes et al., 2013); orange dots are from Alert, Canada (ALT) and Barrow, Alaska (BRW) (<ftp://aftp.cmdl.noaa.gov/>); light blue line is and light green lines are the atmospheric scenarios prepared for the NEEM firn modeling (Buizert et al., 2012) and the CMIP6 experiments (Meinshausen et al. 2017), respectively.

Systematic measurements of atmospheric CH<sub>4</sub> mole fraction began in the 1980s. In Figure 1, CH<sub>4</sub> measurements at two Arctic sites: Barrow, Alaska (BRW) and Alert, Canada (ALT) are shown (orange dots), whose records start in 1983 and 1985, respectively (data provided by National Oceanic and Atmospheric Administration/Earth System Research Laboratory/Global Monitoring Laboratory, NOAA/ESRL/GML). Although some sparse data from the 1970s are available (e.g. Rice et al., 2016), such “direct” measurements provide CH<sub>4</sub> data only since around 1980, which means that some reconstruction methodology is required to infer atmospheric CH<sub>4</sub> mole fraction variations before that time. For this purpose, air extracted from ice cores and firn layers have been measured. Figure 1 also presents CH<sub>4</sub> mole fractions analyzed in ice cores from Greenland (open blue

symbols), such as Eurocore (Blunier et al., 1993), Eurocore and GISP2 (Greenland Ice Sheet Project 2) (Etheridge et al., 1998) and Site J (Nakazawa et al., 1993). These data show fairly good agreements with each other until ~1900, after which the number of data and the consistency among the records are poor. Continuous measurements from NEEM-S1 ice core (Rhodes et al., 2013) presented CH<sub>4</sub> mole fractions before ~1960 (red in Figure 1), but their data are notably higher than the ice core data after ~1850. Therefore, the inconsistency among the different data gaps indicates that the period between ~1900 and ~1980 is not covered reliably either by direct observations or ice core reconstructions.

In comparison to these data, higher-resolution CH<sub>4</sub> data are available from Antarctica (grey in Figure 1). The comprehensive Law Dome ice core and firm data set (Etheridge et al., 1998; MacFarling Meure et al., 2006) almost continuously covers the last 200 years and are well connected to the direct measurements at South Pole (SPO, data provided by NOAA/ESRL/GML) and Cape Grim (CGO) (Etheridge et al., 1998; MacFarling Meure et al., 2006). Such consistency and continuity among the datasets suggests that the Antarctic CH<sub>4</sub> data can serve as a good reference to represent the global atmospheric CH<sub>4</sub> trend over the past ~~centuries~~ two centuries. ~~Buizert et al., (2012) used the Antarctic CH<sub>4</sub> trend with presumed inter-polar difference (IPD) to propose the CH<sub>4</sub> history over Greenland (light blue in Figure 1), which in turn was used to constrain the gas diffusivity profile in firn at the North Greenland Eemian ice Drilling (NEEM) site. In their study, the Arctic CH<sub>4</sub> scenario was constructed by adding IPD to the Law Dome data, where the IPD was assumed to be proportionally correlated with the growth rate of CH<sub>4</sub>. This seems reasonable assumption, given that the IPD and growth rate are both largely subject to changes in emissions from the northern hemisphere (Dlugokencky et al., 2003; Chandra et al., 2021). The Arctic CH<sub>4</sub> scenario by Buizert et al. (2012) is consistent with the direct measurements that started in the 1980s, and ice core reconstructions before ~1900 (Figure 1). It is thus considered as the most likely synthetic atmospheric CH<sub>4</sub> trend for the northern high latitudes, and is treated as a “known” history, by which the diffusivity profiles in firn are tuned in firn-air transport models (Witrant et al., 2012; Trudinger et al., 2013). It is however noted that this scenario has not been validated against independent estimates for the data gap period (from ~1900 to ~1980).~~

Currently, two synthetic data sets for the Arctic historical CH<sub>4</sub> mole fractions are available (see section 3.2). Buizert et al., (2012) prepared Arctic historical trends of mole fractions of atmospheric trace gases including CH<sub>4</sub>, which in turn was used to constrain the gas diffusivity profile in firn at the NEEM site. As seen in Figure 1 (light blue line), the Arctic CH<sub>4</sub> scenario by Buizert et al. (2012) is consistent with the direct measurements that started in the 1980s, and ice core reconstructions before ~1900. Considered as the most likely synthetic atmospheric CH<sub>4</sub> trend for the northern high latitudes, this scenario was treated as a “known” history, by which the diffusivity profiles in firn were tuned in firn-air transport models (Witrant et al., 2012; Trudinger et al., 2013). The other is the composite data set prepared for use in the CMIP6 experiments (Meinshausen et al. 2017). They provide latitudinal monthly gridded fields of various greenhouse gas mole fractions to be consistent with available measurements. It is seen that their scenario for the northernmost latitude (green in Figure 1) follows the NEEM-S1 ice core data set (red). Figure 1 shows that the two synthetic data sets of the historical CH<sub>4</sub> trend are inconsistent in particular for the early 20th century, and it is highlighted in this study that these scenarios have not been sufficiently validated against independent estimates for the data gap period (from ~1900 to ~1980).

In this study, we present a set of mole fractions of CH<sub>4</sub> and other trace gases in firn-air samples collected at the ~~North Greenland Ice Core Project (NGRIP)~~ site. Using the available atmospheric scenarios ~~by Buizert et al. (2012),~~ we simulate the depth profiles of trace gases in the NGRIP firn with our firn-air transport model ~~as well as those in the NEEM firn reported previously (Buizert et al., 2012).~~ We examine a variety of modeling cases for different diffusivity profiles and reconstruct the Arctic atmospheric CH<sub>4</sub> over the late 20th century using the iterative dating approach (Trudinger et al., 2002). The reconstructed CH<sub>4</sub> ~~trend is trends from both firn are~~ evaluated by comparison to the ~~original~~ atmospheric CH<sub>4</sub> ~~scenario and to the NEEM firn air data scenarios.~~ Uncertainty of the Arctic atmospheric CH<sub>4</sub> history for use in firn-air modeling is discussed.

## 2 Experimental method

Firn air was sampled at the Greenland site NGRIP (75°10'N, 42°32'W, 2959 m AMSL) in May–June 2001. Accumulation, surface density, mean temperature and pressure are 179 kg m<sup>-2</sup> yr<sup>-1</sup>, 300 kg m<sup>-3</sup>, 241 K and 680 hPa, respectively. Details of the firn and firn-air sampling have been described elsewhere (Kawamura et al., 2006; Ishijima et al., 2007). At the NGRIP site, two shallow holes (EU and Japanese holes) were drilled (Kawamura et al., 2006; Landais et al., 2006), and the present data are from the firn-air samples collected from the Japanese hole. The total number of air-sampling depths is 24.

Since the technical details are reported in Kawamura et al. (2021), only brief descriptions of relevant data presented in this study are given here. CH<sub>4</sub> mole fractions of the firn-air samples were measured using a gas chromatograph (Agilent 6890, Agilent Technologies Inc.) equipped with a flame ionization detector (GC-FID) at Tohoku University (TU), with a reproducibility of 2 ppb (Umezawa et al., 2014). The CH<sub>4</sub> mole fractions were determined against our working standard gases that were calibrated on the TU1987 CH<sub>4</sub> scale (Aoki et al., 1992; Umezawa et al., 2014; Fujita et al., 2018). The difference between the TU1987 CH<sub>4</sub> scale and the WMO CH<sub>4</sub> mole fraction scale (on which the NEEM CH<sub>4</sub> data were measured) is estimated to be ~0.5 ppb at the current atmospheric CH<sub>4</sub> levels (Fujita et al., 2018). Oyabu et al. (2020) reported that ice core data analyzed on the TU1987 and WMO scales showed good agreement within analytical uncertainties, indicating consistency of both scales, including for the lower mole fractions (e.g. ~700 ppb). It is therefore likely that the difference between both scales is well below the variations of interest in this study, and thus no correction is applied for use of the NGRIP and NEEM firn data.

The firn-air samples were measured for CO<sub>2</sub> and SF<sub>6</sub> mole fractions respectively by using a nondispersive infrared gas analyzer (NDIR) and a gas chromatograph equipped with an electron capture detector (GC-ECD) at TU. The measurement reproducibility is estimated to be 0.02 ppm for CO<sub>2</sub> and 0.09 ppt for SF<sub>6</sub> and mole fractions of both gases are reported on the TU2010 CO<sub>2</sub> and TU2002 SF<sub>6</sub> scales, respectively (Sugawara et al., 2018).

The NGRIP firn-air samples were also analyzed for selected halocarbons (CFC-11, CFC-12, CFC-113 and CH<sub>3</sub>CCl<sub>3</sub>) on the Vacuum Preconcentration and Refocusing-Gas Chromatography-Mass Spectrometry (VPR-GCMS) system, which was developed based on the work by Saito et al. (2006). An aliquot of the sample was transferred into an evacuated canister of ~0.3 L at around ambient pressure (~100 kPa) and the inner pressure of the canister was recorded. The air is extracted by a vacuum

135 pump through a preconcentration trap filled with HayeSep D cooled to  $-135^{\circ}\text{C}$  using a Stirling cooler. The preconcentration  
trap was heated to  $-70^{\circ}\text{C}$  to release major atmospheric constituents and then up to  $100^{\circ}\text{C}$  to transfer the trapped compounds  
to a cryofocusing trap containing Carboxene 1000/Tenax TA at  $-100^{\circ}\text{C}$ . The trap was then heated to  $180^{\circ}\text{C}$  to inject the  
trapped gases onto a PoraBOND Q separation column for subsequent analysis on MS. Mole fractions of individual halocarbons  
are determined against a working standard gas (compressed dry air) that was calibrated against synthetic standards on the  
140 NIES-08 scales.

### 3 Firn-air transport model

Since the gas diffusivity in firn layers is significantly lower than in the atmosphere, the movements of atmospheric constituents  
are driven mostly by molecular diffusion according to their vertical mole fraction gradients under the influence of gravity. In  
general, lighter air components (or isotopologues) diffuse faster under their mole fraction gradients, while heavier components  
145 accumulate in the deeper layers due to the gravitational effect. Hence the depth profiles of trace gas mole fractions in firn are  
determined by the atmospheric histories transferred towards depth in the firn by the molecular diffusion driven by the mole  
fraction gradient and gravity. At the bottom of firn, the air is trapped as bubbles in the ice sheet, which creates slow downward  
motion of firn air.

The firn column can be divided into three zones: a convective zone (CZ), a diffusive zone (DZ) and a lock-in zone (LIZ)  
150 (Sowers et al., 1992; Kawamura et al., 2006; Buizert et al., 2012). In CZ, primarily driven by surface winds and fluctuations  
of atmospheric pressure, air is mixed with the overlying atmosphere (Sowers et al., 1992; Kawamura et al., 2006). The CZ  
thickness at NGRIP is estimated to be below 2 m (Kawamura et al., 2006). In DZ, which is sufficiently isolated from the  
surface turbulence, movement of air is governed by molecular diffusion. Gravitational enrichment according to the barometric  
equation (i.e. linear increases of  $\delta^{15}\text{N}$  of  $\text{N}_2$  and  $\delta^{18}\text{O}$  of  $\text{O}_2$ ) occurs with depth, which stops at the top of LIZ (Sowers et al.,  
155 1992; Schwander et al., 1993; Kawamura et al., 2006). The top of LIZ (lock-in depth) at NGRIP is at depth 63 m (Kawamura  
et al., 2006). In LIZ, advection with the enclosing ice matrix dominates the transport of air, and air parcels are gradually  
isolated as bubbles. Traditionally, it was supposed that high-density impermeable ice layers stop diffusivity in LIZ completely,  
however, recent studies demonstrated finite diffusivity in LIZ (Severinghaus et al., 2010; Buizert et al., 2012; Trudinger et al.,  
2013). The deepest air sampling at NGRIP was successfully made at 77.71 m, and total pore closure is considered in the deeper  
160 layers in our modeling.

#### 3.1 Modeling firn-air transport

We use a one-dimensional diffusion model that has been used for the reconstruction of isotope ratios of  $\text{CO}_2$  and  $\text{N}_2\text{O}$   
(Sugawara et al., 2003; Ishijima et al., 2007). The model is conceptually similar to that developed by Trudinger et al. (1997);  
it is based on a theoretical formation of diffusion (Schwander et al., 1993) and a bubble trapping process (Rommelaere et al.,

165 1997). Air movement in the firn is driven by molecular diffusion and a gravitational effect. Namely, a trace gas flux in firn is expressed by

$$F = -D \left\{ s \frac{\partial}{\partial z} \left( \frac{c}{s} \right) - \frac{mgc}{RT} \right\}, \quad (1)$$

where  $D$  is the effective diffusivity of a trace gas molecule, the variables  $s$ ,  $c$ , and  $T$  are open porosity, trace gas molar concentration, and firn temperature, respectively, and the constants  $m$ ,  $g$ , and  $R$  are the mass number of the trace gas, the acceleration of gravity, and the gas constant, respectively. Vertical advection flux of the trace gas, caused by air trapping at the close-off zone and downward bulk motion of firn, is expressed by using the equation given by Rommelaere et al. (1997). Conservation of the trace gas is given by

$$\frac{\partial c}{\partial t} + \frac{\partial(vc)}{\partial z} + \frac{\partial F}{\partial z} + rc = 0, \quad (2)$$

for the open pore space and

$$175 \quad \frac{\partial c_b}{\partial t} + \frac{\partial(v_f c_b)}{\partial z} - rc = 0, \quad (3)$$

for bubbles. Here  $c$  and  $c_b$  are trace gas molar concentrations in the open pore space and bubbles, respectively. Vertical speed of air in the open pore space  $v$  is distinguished from that of firn itself  $v_f$ . The vertical speed of firn  $v_f(z)$  is simply given by dividing the accumulation rate by the firn density under the assumption of the steady-state densification of firn. At the transition zone where the open pore air is gradually trapped into bubbles, mass conservation is given by using a bubble trapping rate  $r$  ( $s^{-1}$ ), which simply means that a portion of the trace gas molar concentration in the open pore space ( $rc$ ) is added to bubbles. The bubble trapping rate is given as a function of the open porosity, the total porosity, and the vertical speed of firn itself (Rommelaere et al., 1997). The total porosity was calculated from the firn density data. At the transition zone, the total porosity should be divided into the open and closed porosity. The closed porosity  $s_c$  was calculated by the empirical equation given by Schawander (1989).

### 185 3.2 Atmospheric scenarios

To simulate depth profiles of trace gases in firn, atmospheric histories of the target gases are required. In this study, we used atmospheric histories prepared by the NEEM firn-air modeling (Buizert et al., 2012) and by the CMIP6 experiments (Meinshausen et al., 2017) for all the trace gases presented in this study for the NGRIP and NEEM firn ( $CH_4$ ,  $CO_2$ ,  $SF_6$ , CFC-11, CFC-12, CFC-113, HFC-134a,  $CH_3CCl_3$  and  $^{14}CO_2$ ). Since Meinshausen et al. (2017) provides latitudinally gridded datasets, their historical data for the northernmost latitude (82.5° N) are used. Note that the  $^{14}CO_2$  history for CMIP6 is available from another study (Graven et al., 2017), which is also used in this study. The  $^{14}CO_2$  data by Graven et al. (2017) are available in  $\Delta^{14}CO_2$  for three zonal bands (northern hemisphere, tropics and southern hemisphere), and were converted to  $^{14}CO_2$  mole fraction as in Buizert et al. (2012). These atmospheric scenarios (hereafter referred to as the BZ and CMIP6 scenarios) are compared in Figure 2. The BZ (light blue) and CMIP6 (blue) scenarios show compatible historical trends in many trace gases.



195 There are however slight differences in some trace gases between the two scenarios e.g. SF<sub>6</sub> and CFC-12, but we later show  
that these differences do not cause significant biases in reproducing their depth profiles at the NGRIP and NEEM firn sites.  
In contrast, the Arctic CH<sub>4</sub> histories by the two studies differ considerably (Figure 2b). The two CH<sub>4</sub> histories show similar  
trends after 1960, but before this, the data sets diverge the further into the past. This disagreement is also clear in the interpo-  
lar difference (IPD), calculated relative to the CMIP6 histories for Antarctica (right axes). While the BZ scenario shows a gradual  
200 increase in IPD, the CMIP6 scenario indicates almost constant values at ~130 ppb over the 20th century. This difference stems  
from the different methodologies that were used to produce the respective scenarios. As described by Buizert et al. (2012), the  
BZ CH<sub>4</sub> scenario was constructed by adding the presumed IPD to the Antarctic history (the Law Dome data), where the IPD  
was assumed to be proportionally correlated with the growth rate of CH<sub>4</sub>. This seems a reasonable assumption, given that the  
IPD and growth rate are both largely subject to changes in emissions from the northern hemisphere (Dlugokencky et al., 2003;  
205 Ghosh et al., 2015; Chandra et al., 2021). Meinshausen et al. (2017) compiled historical measurement records from the  
worldwide networks as well as Antarctic/Greenland ice core and firn samples and constructed latitudinally gridded datasets of  
various greenhouse gases. For the historical trend of CH<sub>4</sub>, they relied on the data set from the NEEM-S1 ice core by Rhodes  
et al. (2013) to produce the atmospheric histories for the northern hemisphere. They used the 5-yearly averaged values with  
outliers removed to represent lower bounds of the raw data points as shown in Figure 1. Note that the Rhodes et al. (2013) data  
210 set was not available when the BZ scenario was constructed. Therefore, CH<sub>4</sub> is the only compound, with an available  
atmospheric history, which shows a clear disagreement, thus highlighting the limitation of our current understanding of its  
atmospheric historical trend for the northern hemisphere. Conversely, this study assumes that the atmospheric scenarios for  
other trace gases are known with sufficient accuracy. The scenarios of the individual trace gases have inherent uncertainties,  
but the comparisons of the two scenarios indicate that the other gases are at least better known than CH<sub>4</sub>.

215

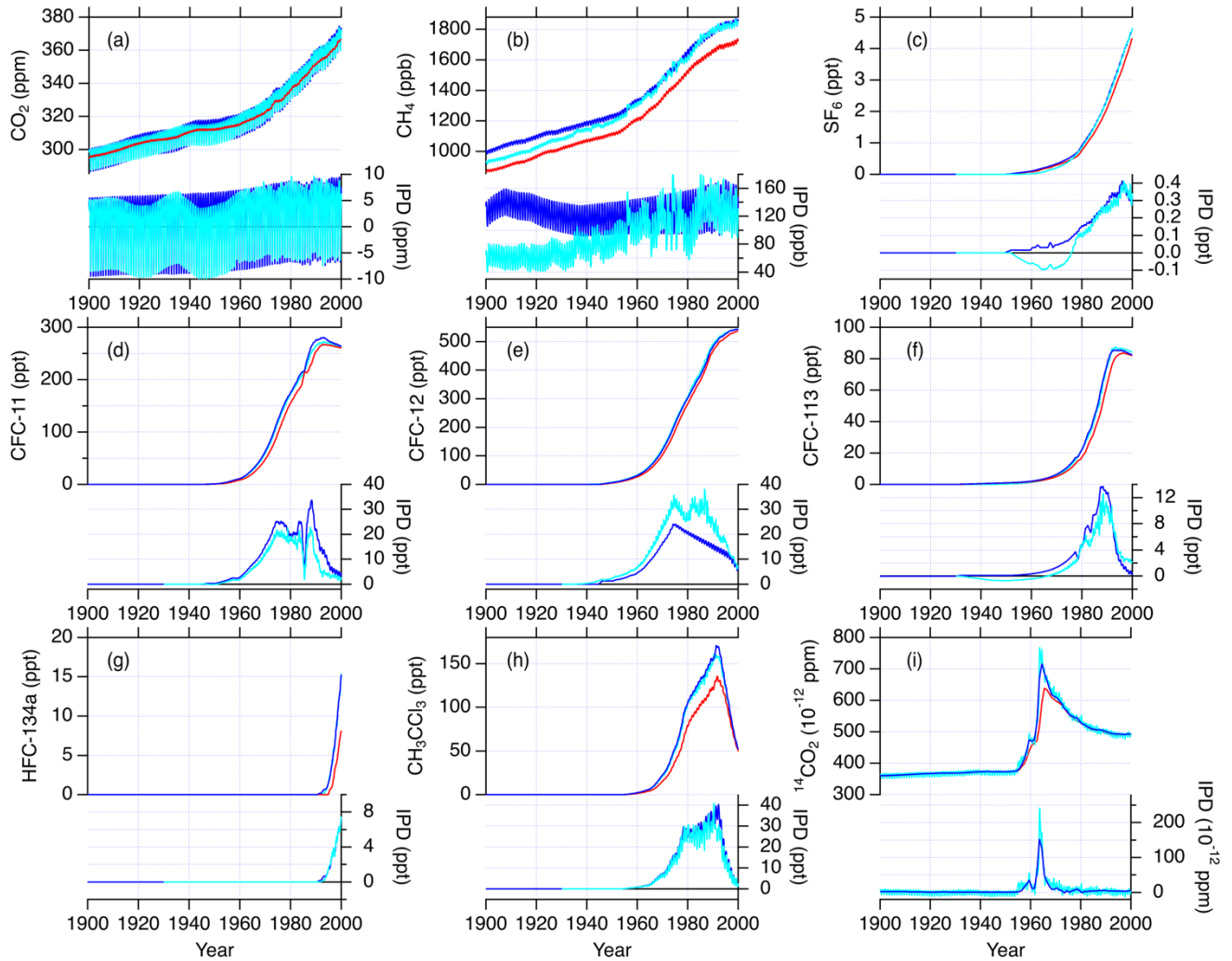


**Figure 2: Atmospheric scenarios of various trace gases used in this study. The Arctic histories prepared for the NEEM firn-air modeling (Buizert et al., 2012) are in light blue. The Arctic and Antarctic histories for CMIP6 (Meinshausen et al., 2017) are in blue and red, respectively. For  $^{14}\text{CO}_2$ , the CMIP6 historical data are from Graven et al. (2017). The inter-polar differences (IPDs) calculated from the Arctic histories with respect to the Antarctic CMIP6 histories are also shown (right axes).**

### 3.3 Effective diffusivity

We follow the previous firn-air studies in which the effective diffusivity in firn is optimized with an iterative method so as to minimize the difference between the simulated and observed depth profiles of  $\text{CO}_2$  (Sugawara et al., 2003; Ishijima et al., 2007). ~~An~~ In these previous studies, an initial guess of the effective diffusivity for  $\text{CO}_2$ ,  $D_{\text{init}}(z)$ , was calculated by:

$$D_{init}(z) = D_0 \left( \frac{T}{253} \right)^{1.85} \left( \frac{1013}{p} \right) \{1.7s(z) - 0.2\}, \quad (4)$$

where  $s(z)$  and  $D_0$  represent the open porosity at a depth  $z$  and the diffusion coefficient of  $\text{CO}_2$  at 253 K and 1013 hPa, respectively.  $D_0$  was set to  $1.247 \times 10^{-5} \text{ (m}^2 \text{ s}^{-1}\text{)}$  according to Trudinger et al. (1997). The bulk density was determined by measuring the dimension and weight of cylindrically cut firn core samples (Kawamura et al., 2006). The effective diffusivity

of  $\text{CO}_2$  thus obtained, was converted to those of other trace gases by multiplying by scaling factors from Buizert et al. (2012). Therefore, the depth profile pattern of the effective diffusivity is identical among all gases, but the magnitude is gas-dependent due to the scaling factors. In this study, the effective diffusivity profile prepared for the NGRIP firn by Ishijima et al. (2007)

is referred to as the initial diffusivity and it was modified to improve the reproducibility of our newly measured trace gas profiles. For simulating trace gas profiles for the NEEM firn, we began with the effective diffusivity profiles available from

Buizert et al. (2012). Those effective diffusivity profiles, which were originally optimised for individual firn-air transport models that participated in that study, were modified and used for simulating the various trace gas profiles reported for the NEEM firn. The various diffusivity profiles were constructed by modifying the original profiles at a certain range of depths in a stepwise manner. Although this simple method does not guarantee identification of a best-match profile, we are confident that an acceptable range of the diffusivity profile is satisfactorily constrained. (section 4). We eventually prepared 100 different

sets of diffusivity profiles so as to cover a considerable range of diffusivity. Each set of the diffusivity profiles was evaluated based on the root mean square deviation (RMSD) between the model and data according to Buizert et al. (2012). All sets of effective diffusivity profiles for the NGRIP and NEEM firn sites are shown in Figure 3 (top and bottom panels, respectively). The different colors of the diffusivity profiles will be explained later. As shown in the figure, we examined a considerable range of effective diffusivity for different firn layers at both NGRIP and NEEM firn sites. Those diffusivity profiles were

evaluated against the observed trace gas profiles, which were regarded as constraints. Note that, in the evaluation, the atmospheric scenarios of the trace gases (except  $\text{CH}_4$ ) are assumed to be known with sufficient accuracy to infer a range of acceptable diffusivity profiles that reproduce the depth profiles of the firn-air composition.

3.3 Performance of the firn air transport model

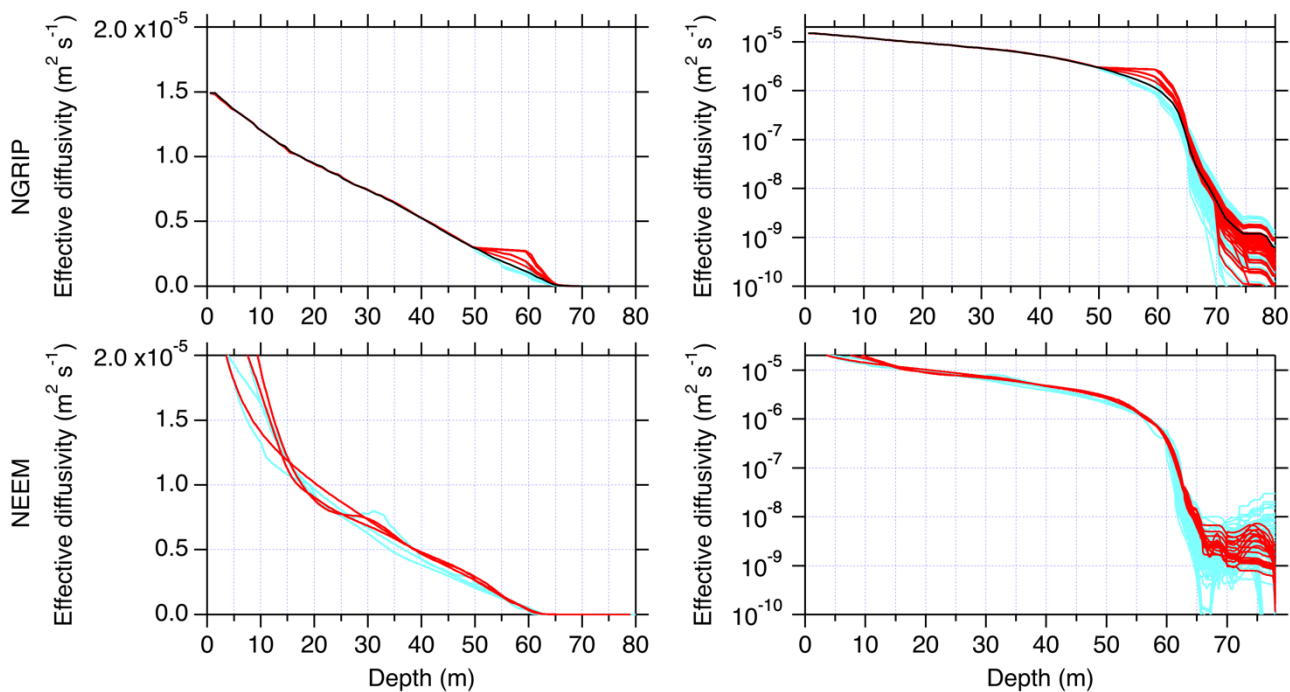
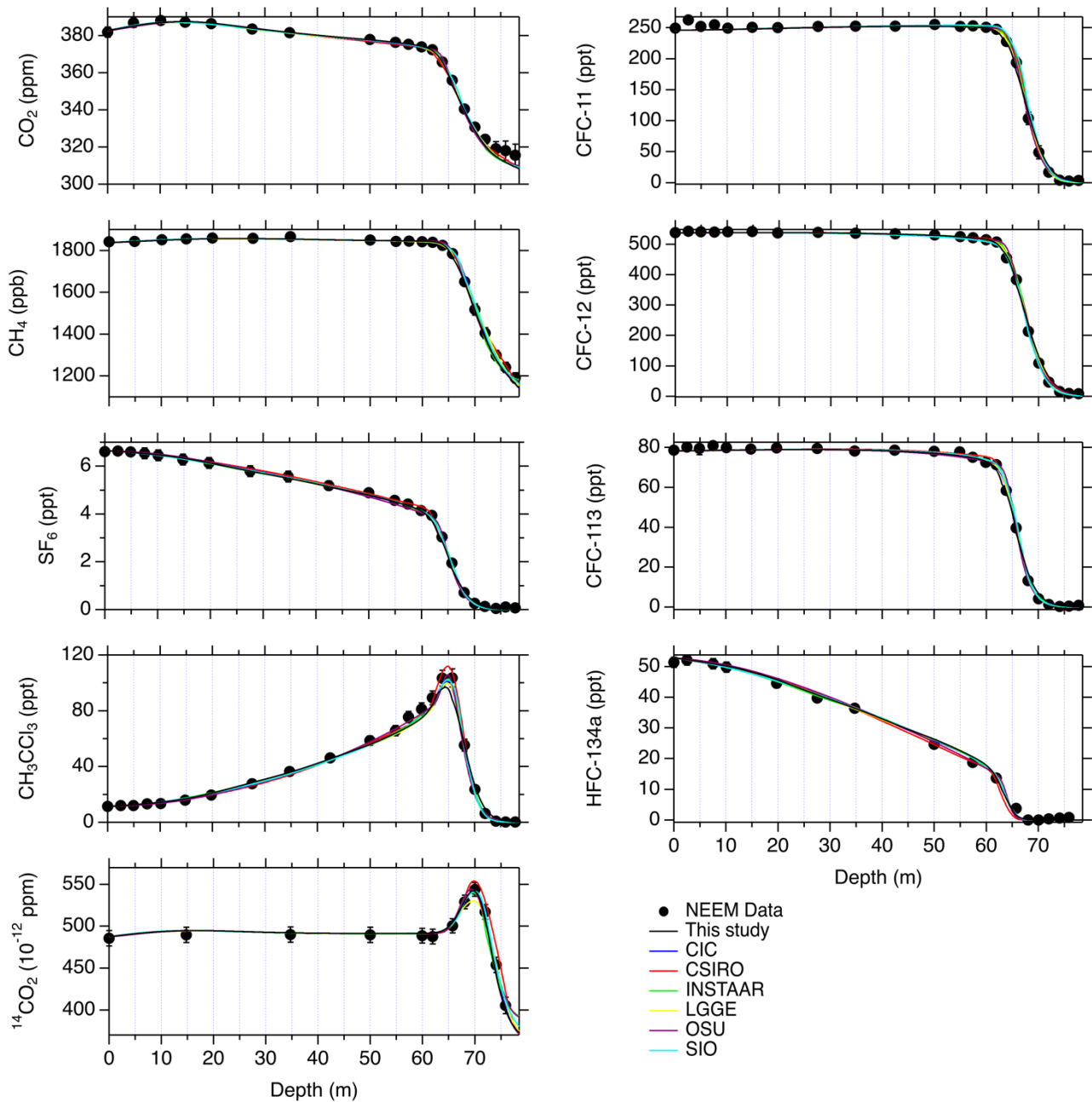


Figure 3: The 100 sets of effective diffusivity profile of CO<sub>2</sub> in the NGRIP (top panels, left panel on a linear scale and right panel on a log scale) and NEEM firn (bottom panels). The initial diffusivity profile (Ishijima et al., 2007) is shown in black (NGRIP only) and modified diffusivity profiles are in colors. The diffusivity profiles whose corresponding mole fraction profiles have RMSD values of <1.0 are colored red and the others light blue.

3.4 Performance of the firn-air transport model

To validate our firn-air transport model, we simulated depth profiles of various trace gases in the NEEM firn. Our model did not participate in the model intercomparison study using the NEEM data (Buizert et al., 2012). In this simulation, we employed the atmosphericBZ scenarios prepared by Buizert et al. (2012) as per their model intercomparison. The diffusivity profile optimized for the CIC (Center for Ice and Climate, Niels Bohr Institute, University of Copenhagen) model was tuned for our model. The simulated depth profiles of various compounds the nine trace gases are presented in Figure 24 and compared with those by other models presented in Buizert et al. (2012). The results confirm that the performance of our model is comparable to those by other groups. As a measure of the model performance, Buizert et al. (2012) compared root mean square deviation (RMSD) between the model and data, which ranged from 0.73 to 0.92 for the six participating models. Following the same approach, our model yields the RMSD value of 0.83 of for the NEEM EU borehole for the NEEM EU borehole. This RMSD value was achieved with an effective diffusivity profile that was prepared by modifying the profile originally optimised for the CIC (Centre for Ice and Climate) model at a certain range of depths. Note that the RMSD value

here was calculated including CH<sub>4</sub> as per Buizert et al. (2012), but, as described in section 3.5, CH<sub>4</sub> is excluded in calculation of RMSD in the following sections.



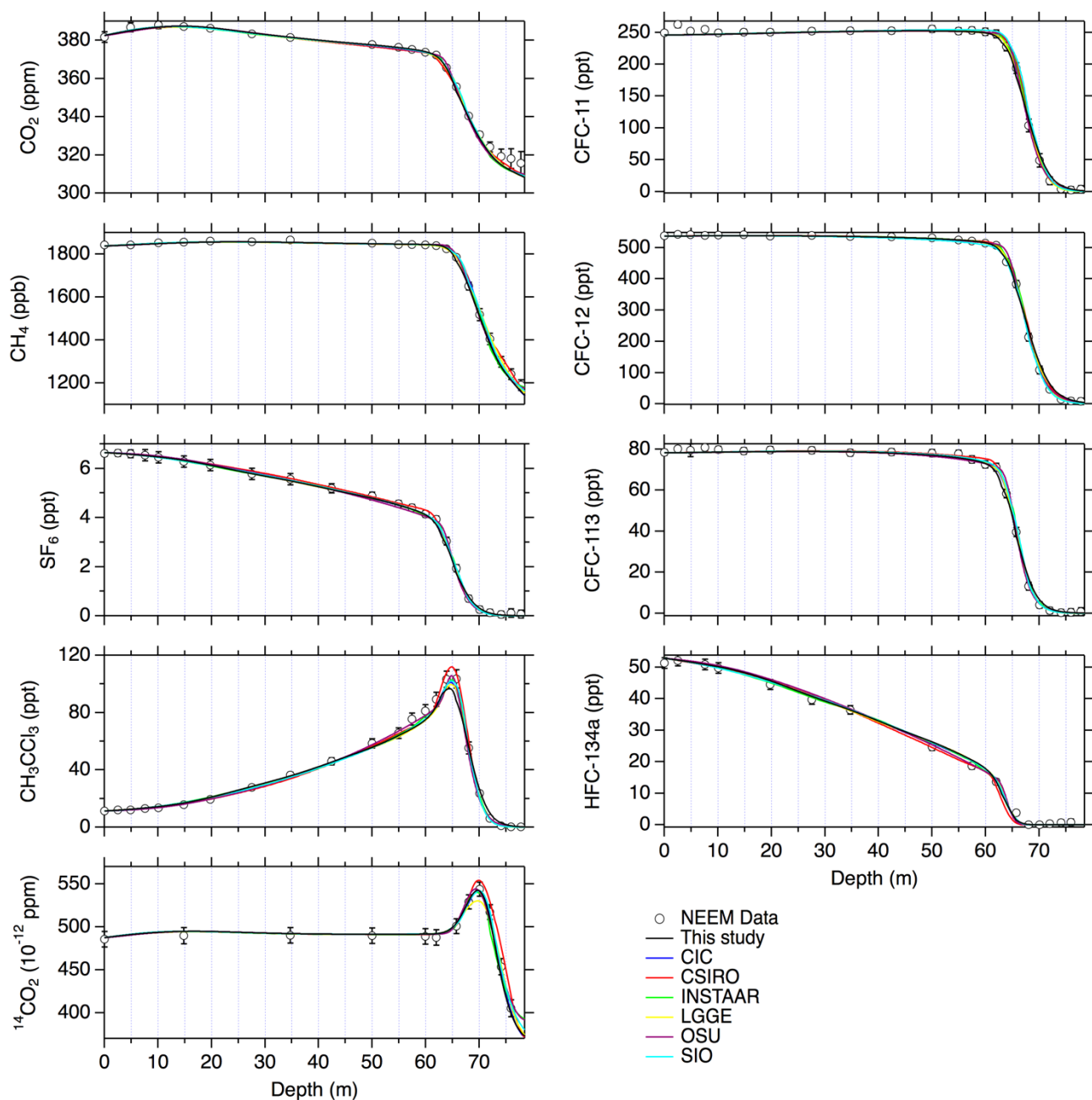


**Figure 24:** Modeled depth profiles of various compounds in the NEEM firn. **Open**Closed circles in black are the observed data with uncertainty estimated by Buizert et al. (2012). Our model results are shown in black solid lines and results from other models are in colors. Different models are labeled by institutions according to Buizert et al. (2012): CIC (Centre for Ice and Climate), CSIRO (Commonwealth Scientific and Industrial Research Organization), INSTAAR (Institute of Arctic and Alpine Research), LGGE (Laboratoire de Glaciologie et Géophysique de l'Environnement), OSU (Oregon State University) and SIO (Scripps Institution of Oceanography).

### 3.4.5 Modeling procedure

280 Our modeling procedure for reconstructing the atmospheric histories of ~~trace gases~~CH<sub>4</sub> was as follows:

(1) To represent atmospheric trace gas trends in the Arctic region, we began by employing the two sets of atmospheric scenarios prepared for the NEEM firn air modeling (Buizert et al., 2012) for all the trace gases presented in this study (CH<sub>4</sub>, CO<sub>2</sub>, SF<sub>6</sub>, CFC-11, CFC-12, CFC-113 and CH<sub>3</sub>CCl<sub>3</sub>), (section 3.2). The firn transport model calculates depth profiles of ~~these~~the various trace gases ~~in~~at the NGRIP and NEEM firn ~~with~~sites using the ~~initial~~large set of modified ( $N=100$ ) effective diffusivity/diffusivities described in section 3.2.

(2) ~~We examined the different sets of diffusivity profiles so as to improve overall reproducibility of the modeled profiles of the six trace gases except CH<sub>4</sub>. In other words, we regarded these six trace gases as constraints to the 3. The simulation case with each diffusivity profile. Note that this step assumes that the atmospheric histories of the six gases are known with sufficient accuracy to infer a range of acceptable diffusivity profiles that reproduce the depth profiles of the firn air composition. We prepared 100 different sets of modified diffusivity profiles, and the overall model-data agreement for each set was evaluated based on RMSD. As we aim to estimate the historical atmospheric trend of CH<sub>4</sub>, the RMSD-based evaluations were made using all of the available trace gas data, excluding CH<sub>4</sub>. In the RMSD calculation, we used the measurement uncertainties of 0.2 ppm for CO<sub>2</sub>, 0.2 ppt for SF<sub>6</sub>, 1.1 ppt for CFC-11, 3.3 ppt for CFC-12, 0.6 ppt for CFC-113 and 3.2 ppt for CH<sub>3</sub>CCl<sub>3</sub> for the NGRIP firn. For the NEEM firn, we employed the uncertainties provided by Buizert et al. (2012). It should be noted that the present study does not follow the RMSD of the six gases uncertainty estimation as done by Buizert et al. (2012). They indicated that uncertainties in the atmospheric scenarios as well as measurement uncertainties are the two largest contributors to the total uncertainties for individual data points for the NEEM firn. We consider that the uncertainties in the atmospheric scenarios are appreciably examined through comparisons of series of simulations using the two independent scenarios.~~

(3) ~~We ran the model with the 100 different sets of diffusivity profiles to calculate the depth profile of CH<sub>4</sub>. Note that, based on the earlier steps~~step, we know the diffusivity profiles that generate reasonable firn-air profiles for the ~~six~~trace gases other than CH<sub>4</sub>. Every diffusivity profile was used in combination with the firn-air CH<sub>4</sub> data for reconstructing an atmospheric CH<sub>4</sub> history. We employed an iterative dating approach (Trudinger et al., 2002) where the initial atmospheric scenario (the BZ scenario) was modified to improve model reproducibility of the CH<sub>4</sub> depth profile (see below). The corrected atmospheric CH<sub>4</sub> scenarios were then compared to the ~~initial scenario~~original scenarios (BZ and CMIP6) for further discussion.

305 The iterative dating for CH<sub>4</sub> was performed as follows:

(4) ~~Depth profile of CH<sub>4</sub> was calculated with the initial atmospheric CH<sub>4</sub> scenario.~~  
(2) ~~Effective~~(I) The modeled CH<sub>4</sub> mole fraction, calculated in step I, was compared to the input atmospheric CH<sub>4</sub> scenario, and effective age at each sampling depth was ~~calculated so that~~determined as the time when the modeled CH<sub>4</sub> mole fraction, at that depth, agreed with a value in the atmospheric CH<sub>4</sub> scenario. It is noted that the smoothing spline curve applied to the BZ CH<sub>4</sub> scenario was used for calculation of the effective age, as the input scenario with seasonal variation (Figure 2) would not allow the effective age to be uniquely determined.



(~~3~~III) A new atmospheric CH<sub>4</sub> scenario was constructed by assigning the observed CH<sub>4</sub> mole fraction, at each depth, to the effective age determined in step II. The observed CH<sub>4</sub> versus the effective age data set was interpolated by a smoothing spline function and it is considered as a revised atmospheric CH<sub>4</sub> scenario.

(~~4~~IX) Depth profile of CH<sub>4</sub> was again calculated with the revised atmospheric CH<sub>4</sub> scenario constructed in step III.

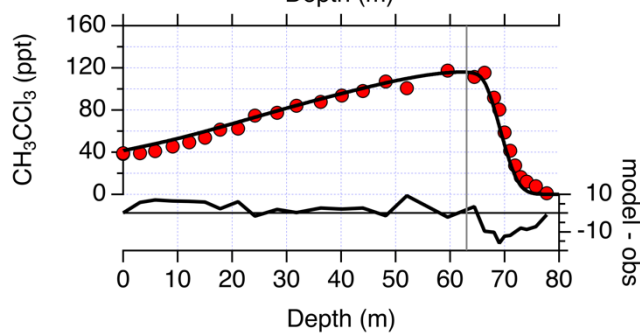
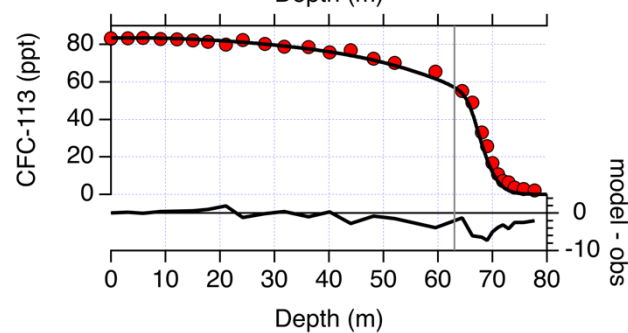
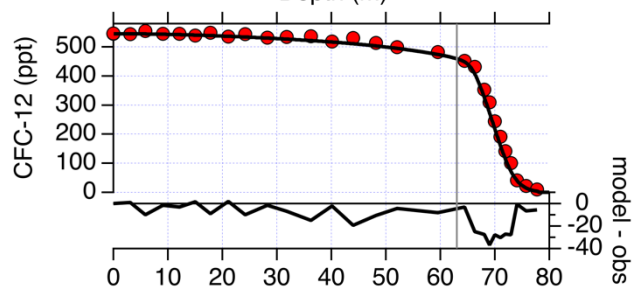
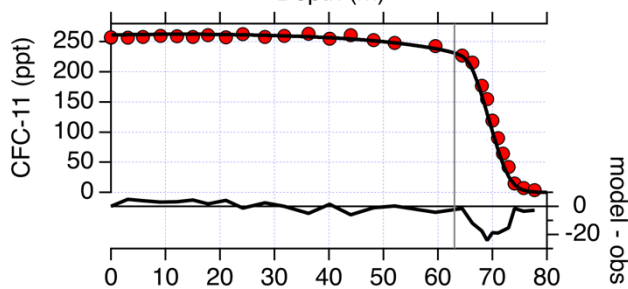
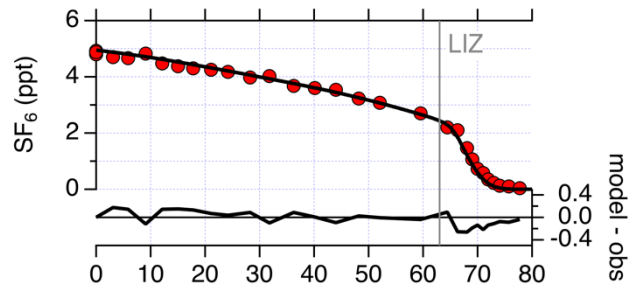
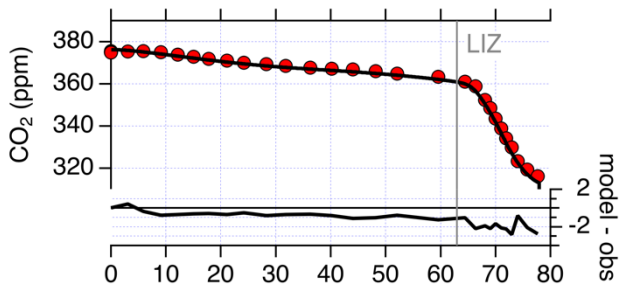
(~~5~~X) The above steps ~~2–4II–IX~~ were repeated until the model-data difference converged within an acceptable range (typically after a few iterations) (Trudinger et al., 2002; Ishijima et al., 2007). In this study, we made five iterations for each modified diffusivity case as we confirmed sufficient convergence of the result.

## 4 Result

### 4.1 Initial and modified diffusivity simulations

Figure ~~3~~5 presents the ~~initial~~ simulation results with the initial diffusivity in comparison to the observed profiles for the six trace gases excluding CH<sub>4</sub> (CO<sub>2</sub>, SF<sub>6</sub>, CFC-11, CFC-12, CFC-113 and CH<sub>3</sub>CCl<sub>3</sub>) for the NGRIP firm. As seen in this figure, measured profiles of these trace gases (except CH<sub>3</sub>CCl<sub>3</sub>) show gradual decreases with depth in the DZ and sharp decreases in the LIZ. In contrast, CH<sub>3</sub>CCl<sub>3</sub> increases with depth in the DZ and sharply decreases in the LIZ. The difference of the depth profile pattern among species is due to their different historical atmospheric trends. It is known that the atmospheric mole fractions of the five trace gases (CO<sub>2</sub>, SF<sub>6</sub>, CFC-11, CFC-12 and CFC-113) have increased monotonically since the mid 20th century (Sturrock et al., 2002; Martinerie et al., 2009). In contrast, CH<sub>3</sub>CCl<sub>3</sub> has increased until the early 1990s and has decreased since then (Sturrock et al., 2002; Rigby et al., 2017~~–~~), which is also observed in Figure 2. Our simulation reproduces the observed depth profiles of these six trace gases in the NGRIP firm fairly accurately ~~with~~using the ~~atmospheric~~BZ scenarios ~~prepared for modeling the NEEM firn air (Buizert et al., 2012).~~





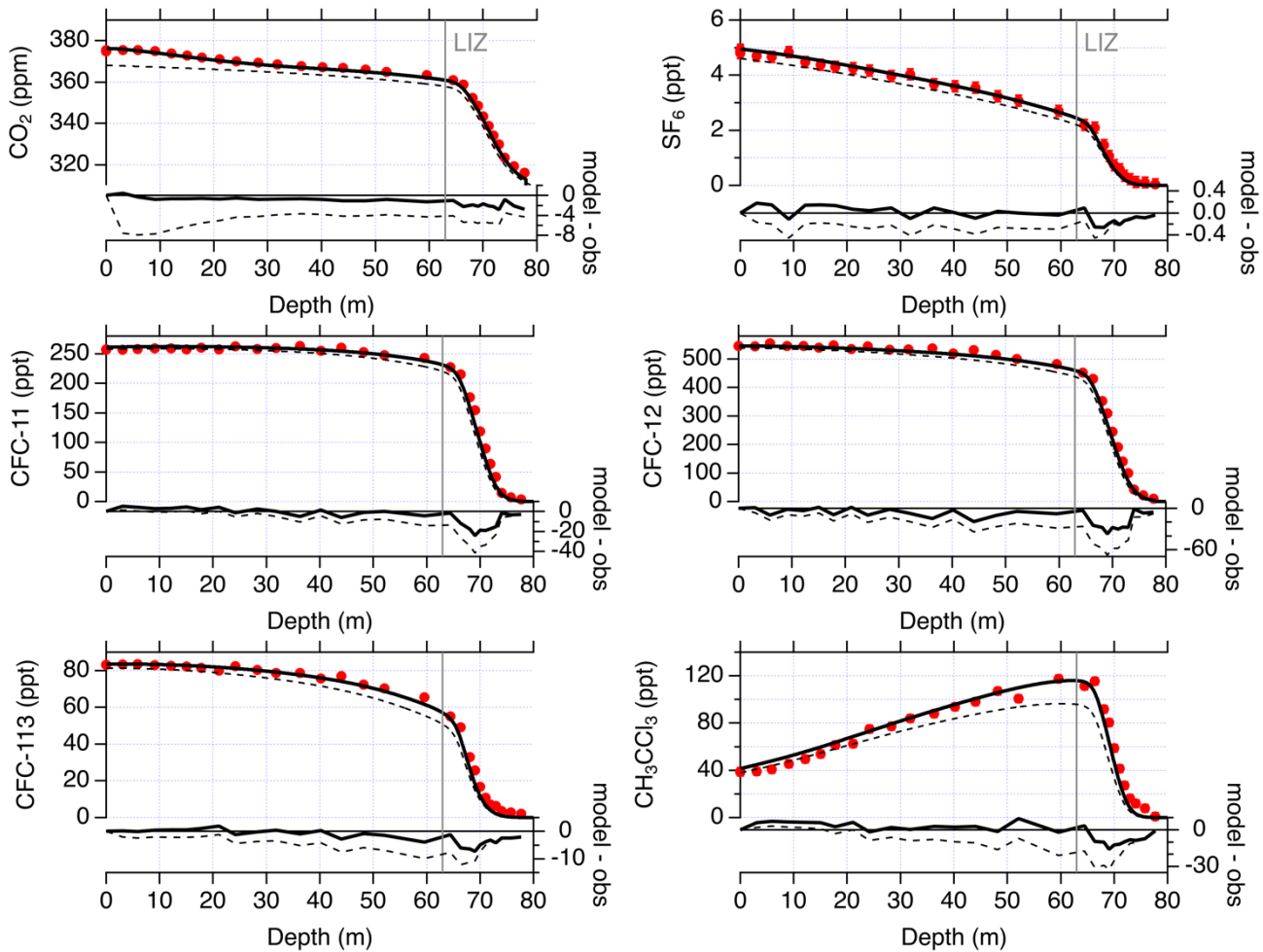


**Figure 35:** Depth profiles of  $\text{CO}_2$ ,  $\text{SF}_6$ , CFC-11, CFC-12, CFC-113 and  $\text{CH}_3\text{CCl}_3$  in the NGRIP firn. The measurement and model results are shown by red circles and black solid lines, respectively (left axis). The measurement uncertainties are shown as vertical error bars though in many cases they are smaller than the circle sizes. **Black solid lines show the modeled profiles with the initial diffusivity and the BZ scenarios. The black dashed lines indicate the profiles calculated with the atmospheric scenarios for Antarctica (red lines in Figure 2).** The model-data differences are also shown (right axis). The vertical solid line in each panel indicates the upper depth of LIZ.

It is interesting to note that the depth profiles of  $\text{CH}_3\text{CCl}_3$  at NGRIP and NEEM are remarkably different. Whereas the NEEM data show a relatively sharp  $\text{CH}_3\text{CCl}_3$  peak in the LIZ (~65 m, Figure 24), NGRIP does not show such a narrow peak. This is due to the timing of firn-air sampling i.e. 2001 for NGRIP and 2008 for NEEM. When the NGRIP firn air was sampled, the signal of the maximum atmospheric  $\text{CH}_3\text{CCl}_3$  in the early 1990s had only reached near the top of the LIZ at the site, thereby formulating the relatively gentle changes at the shallower depths. On the other hand, seven years later at the NEEM site, such a signal was found deeper in the LIZ where the age of air changes rapidly with depth in both deeper and shallower sides. We

emphasize that, despite the differences in the depth profiles of  $\text{CH}_3\text{CCl}_3$  at the two sites, our simulations reproduce both profiles measured at both sites well, using the same atmospheric  $\text{CH}_3\text{CCl}_3$  scenario.

Figure 35 shows that the model-data difference increases in the LIZ for all the trace gases. In particular, the model-data difference is pronounced as a dip around 70 m for all trace gases, implying that the mismatches may originate in a common factor in the modeling e.g. depth profile of diffusivity. To examine the impact of diffusivity modification on the simulated depth profiles and their agreements with the data, we prepared 100 sets of modified diffusivity profiles (Figure 4). The various diffusivity profiles were constructed by modifying the original profile at certain range of depths in a stepwise manner. It was found that, to reduce the model-data difference in the LIZ (Figure 3), the diffusivity needs to be increased in the shallower layers than compared with the top LIZ i.e. 50–65 m. The diffusivity was also modified in the deeper layers (>65 m) and simulations were made accordingly.

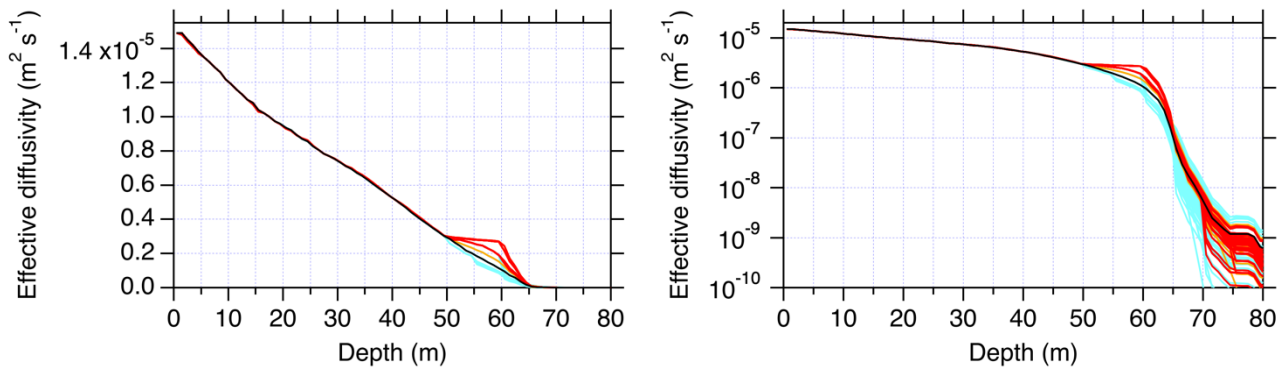


**Figure 4: The 100 sets of effective diffusivity profile of  $\text{CO}_2$  in the NGRIP firn (colored, left panel on a linear scale and right panel on a log scale). The original diffusivity profile is shown in black. See text for colors of the modified diffusivity profiles.**

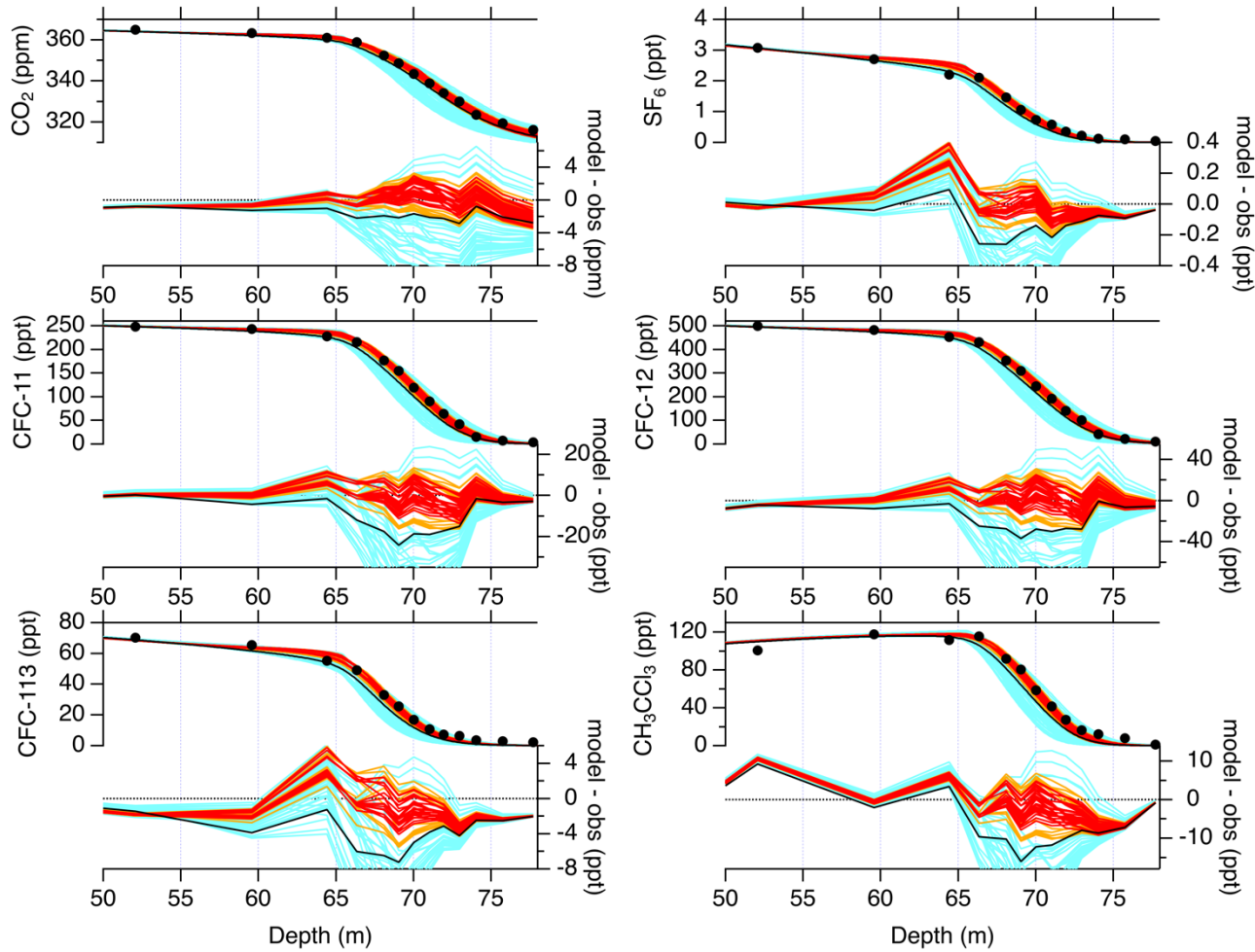
To examine the sensitivity of the trace gas depth profiles to the IPD, we calculated depth profiles that would be expected if the Antarctic atmospheric scenarios (red lines in Figure 2) are given for the NGRIP firn. This sensitivity experiment shows that IPD causes significant biases larger than the measurement precisions of the respective trace gases. We calculated the difference between the simulations for the BZ scenario (solid line) and the Antarctic scenario (dashed line) and found that sensitivities to the IPD for these six trace gases are no more than 20 times the respective measurement uncertainties. Such relative sensitivities of these suite of gases to the IPDs are much smaller than that of  $\text{CH}_4$ , which reaches 40 times the measurement uncertainty. The  $\text{CH}_4$  simulation with the Antarctic scenario for the NGRIP firn resulted in the depth profile >100 ppb less than the original simulation (dotted lines in Figure 8), showing the pronounced impact on  $\text{CH}_4$ .

The simulated profiles for depths deeper than 50 m using the 100 diffusivity profiles are presented for the six trace gases (Figure 56). In this figure, the modeling results with the modified diffusivity profiles are shown in colors on the left axis, and

375

the model-data differences of the respective cases are plotted on the right axis. It is clear that the model-data differences could be significantly reduced with some diffusivity cases. ~~We calculated RMSD in the same manner as Buizert et al. (2012) with the measurement uncertainties of 0.2 ppm for CO<sub>2</sub>, 0.2 ppt for SF<sub>6</sub>, 1.1 ppt for CFC-11, 3.3 ppt for CFC-12, 0.6 ppt for CFC-113 and 3.2 ppt for CH<sub>3</sub>CCl<sub>3</sub>.~~ The RMSD values are as little as 0.51 for a particular case. In Figure 46 and following associated figures, the model results with a RMSD of <0.75 and <1.0 are colored red and orange, respectively, and other cases are colored light blue.

380



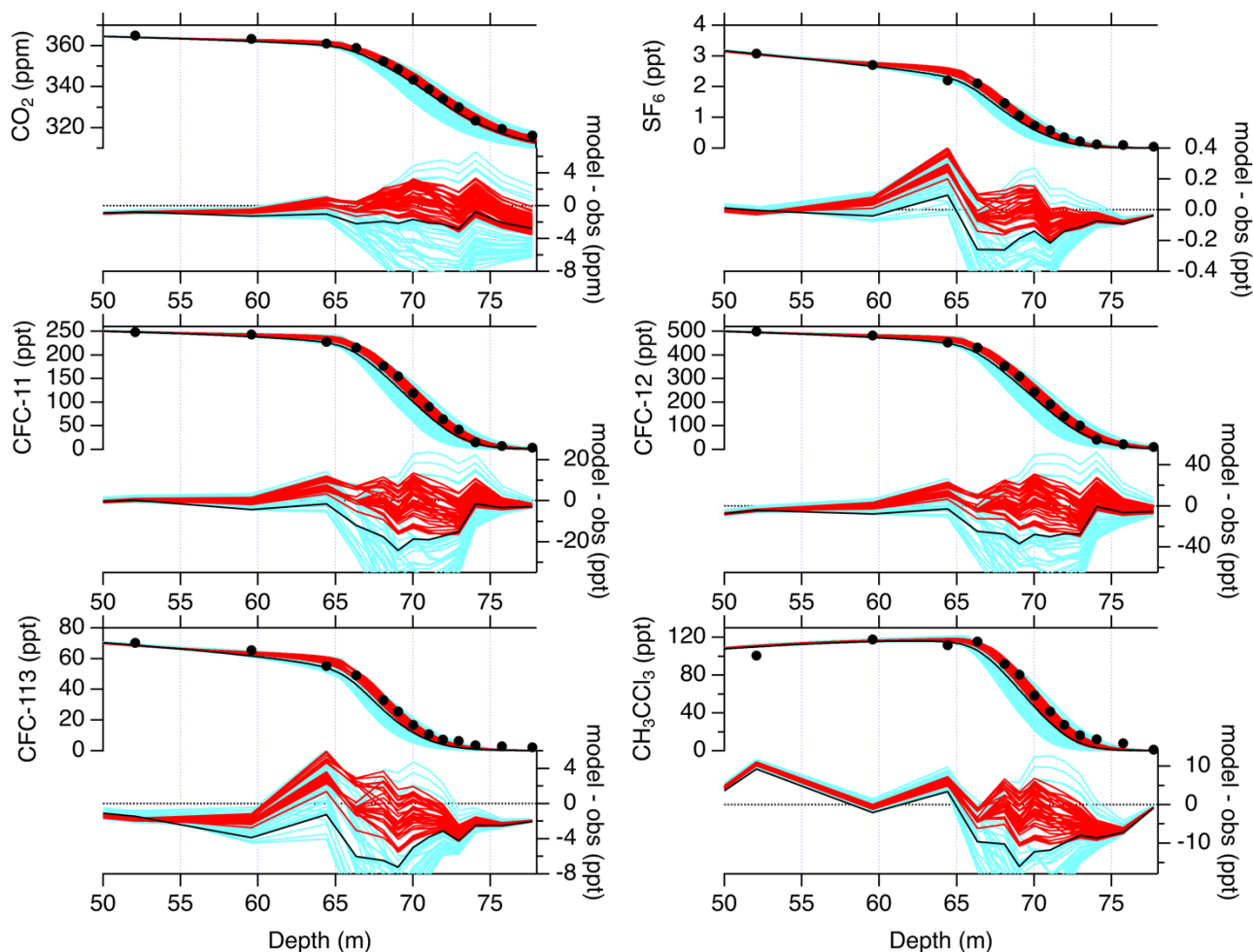
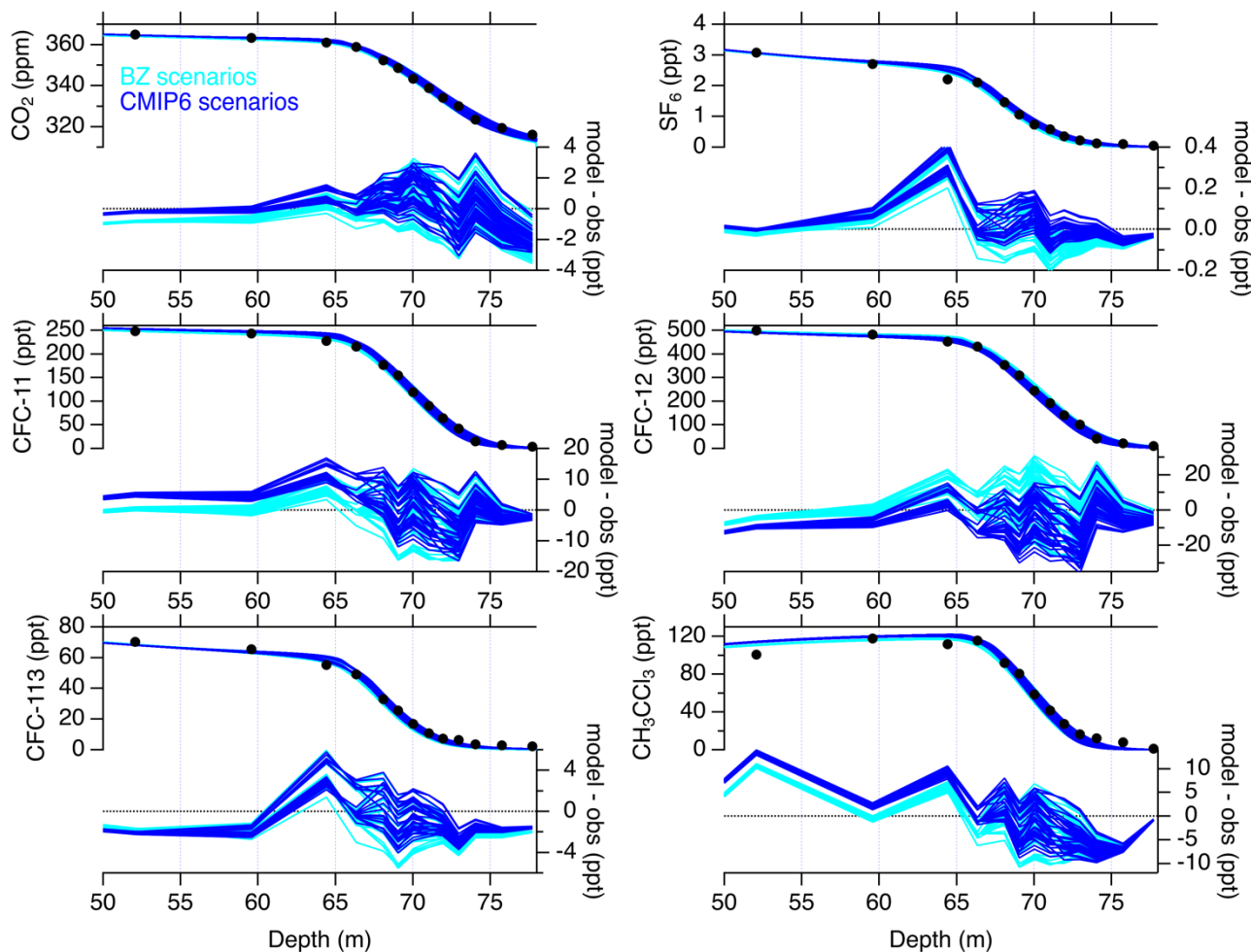


**Figure 56:** Depth profiles of the six trace gases below 50 m depth in the NGRIP firn. Black circles indicate the measurements and solid lines in colors are the model results with different diffusivity profiles and the BZ scenarios (left axis). Black lines are modeled results with the initial diffusivity. Also shown are the model-data differences (right axis). See text for difference in line colors.

Likewise, depth profiles of  $\text{CH}_4$  are shown in Figure 6. These calculations were made with the 100 diffusivity profiles and the atmospheric  $\text{CH}_4$  scenario for the NEEM firn air modeling (Buizert et al., 2012). In Figure 7, modeled depth profiles with different sets of the atmospheric scenarios (BZ and CMIP6) are compared. For simplicity, only the results with RMSD of  $<1.0$  are presented. This figure shows that the differences in the atmospheric histories (Figure 2) produces relatively small differences in the depth profiles in the firn. There are small offsets due to the differences of the histories in some gases; difference in the  $\text{SF}_6$  history before 1980 ( $<0.2$  ppt) corresponds to the small ( $<0.1$  ppt) offsets below 65 m; significant differences in the histories of CFC-11 ( $<10$  ppt) and CFC-12 ( $<20$  ppt) for 1960–1990 resulted in the overall offsets (roughly  $<5$  and  $<10$  ppt, respectively) below 50 m; difference in the  $\text{CH}_3\text{CCl}_3$  history ( $<10$  ppt) in the early 1990s produced the

395

offsets (~3 ppt) above 66 m. The smaller offsets in the calculated depth profiles than in the input atmospheric scenarios are due to the smoothing effect of diffusion in the firn layers. We calculated the difference between the modeled profiles with the two scenarios for individual diffusivity cases and found that those differences in the LIZ are within the measurement precisions for SF<sub>6</sub>, CFC-113 and CH<sub>3</sub>CCl<sub>3</sub>. They are a bit larger for CO<sub>2</sub>, CFC-11 and CFC-12, which are up to five times the respective measurement precisions. The largest impact of the scenario difference occurs in CH<sub>4</sub>. In the LIZ, the difference between depth profiles with the two scenarios reaches to 5–10 times the measurement precision (see Figure 8).



400

**Figure 7: Same as Figure 6, but for comparison of the modeled profiles with different atmospheric scenarios of BZ and CMIP6 in light blue and blue, respectively. Only the simulation results with RMSD values of <1.0 are shown.**

405

Modeled depth profiles of CH<sub>4</sub> are shown in Figure 8. These calculations were made with the 100 diffusivity profiles and the atmospheric CH<sub>4</sub> scenarios of BZ (left) and CMIP6 (right). It is interesting to note that the characteristics of the model-data difference for CH<sub>4</sub> are different from those for the other six trace gases- (Figure 6). For the other trace gases- (Figure 5), the



initial simulation showed increased model-data differences around 70 m, and they were reduced with some modified diffusivity profiles. For CH<sub>4</sub>, the model run with the ~~original~~initial diffusivity profile of the BZ scenario reproduces the observed CH<sub>4</sub> profile quite well down to ~73 m, but significantly overestimates by >20 ppb for the lowest three depths (the black solid line) ~~in the left panel~~. Using the modified diffusivity profiles that allowed better agreements for the other six trace gases (~~orange and red lines~~), ~~we actually find larger model-data CH<sub>4</sub> difference than in the initial simulation~~ red lines), we find larger model-data CH<sub>4</sub> differences than in the initial simulation. These features are commonly seen for the simulation results with the CMIP6 scenario (right panel), but the overestimate in the LIZ is more pronounced, because the CH<sub>4</sub> mole fractions for the early to mid 20th century are higher in the CMIP6 than in the BZ scenario. As described earlier, the difference of depth profiles with the two scenarios exceeds 30 ppb in some diffusivity cases, ten times the measurement precision. Figure 8 also shows the depth profiles which would be expected when the Antarctic CH<sub>4</sub> scenario is used to the firm model (dashed line). The calculated profiles are aligned ~120 ppb below the simulations with the Arctic scenarios, illustrating the large impact of IPD on the CH<sub>4</sub> profile in the Arctic firm.

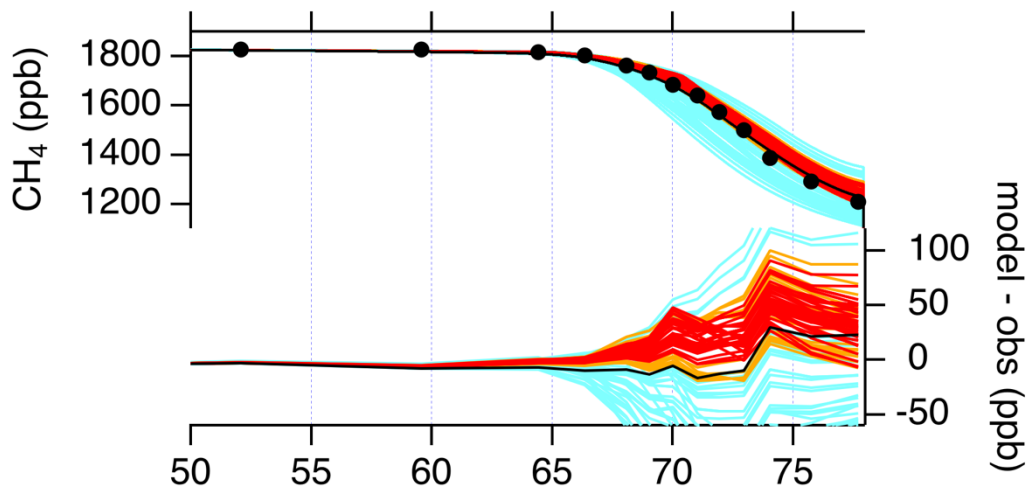
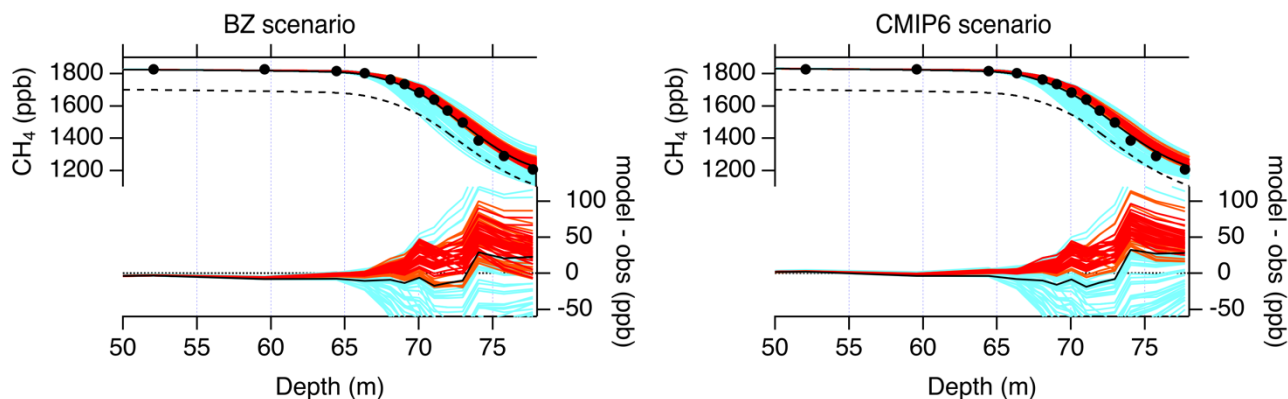


Figure 6: Same as Figure 5, but for CH<sub>4</sub>.



**Figure 8: Same as Figure 6, but for CH<sub>4</sub>. Simulation results with the atmospheric scenarios of BZ and CMIP6 are shown in left and right panels, respectively. The black dashed lines indicate the profiles calculated with the atmospheric scenarios for Antarctica (red line in Figure 2).**

In addition to the above simulations for the NGRIP firn, we examined the impact of the difference of the atmospheric scenarios on the depth profiles for the NEEM firn. In Figure 9, comparisons between simulations with the different scenarios for the nine trace gases including CH<sub>4</sub> are presented. We found some common characteristics at the NGRIP and NEEM firn sites. While the difference between the simulations with the two scenarios are relatively small for most trace gases, the large difference between the CH<sub>4</sub> scenarios (i.e. higher CH<sub>4</sub> mole fraction in the CMIP6 scenario, see Figure 2) produces enlarged overestimate in the LIZ (> 63 m) in the modeled profiles with the CMIP6 scenario. In the LIZ, the difference of the depth profiles with the two scenario exceeds 30 ppb, being comparable to the magnitude observed in the NGRIP firn (Figure 8).



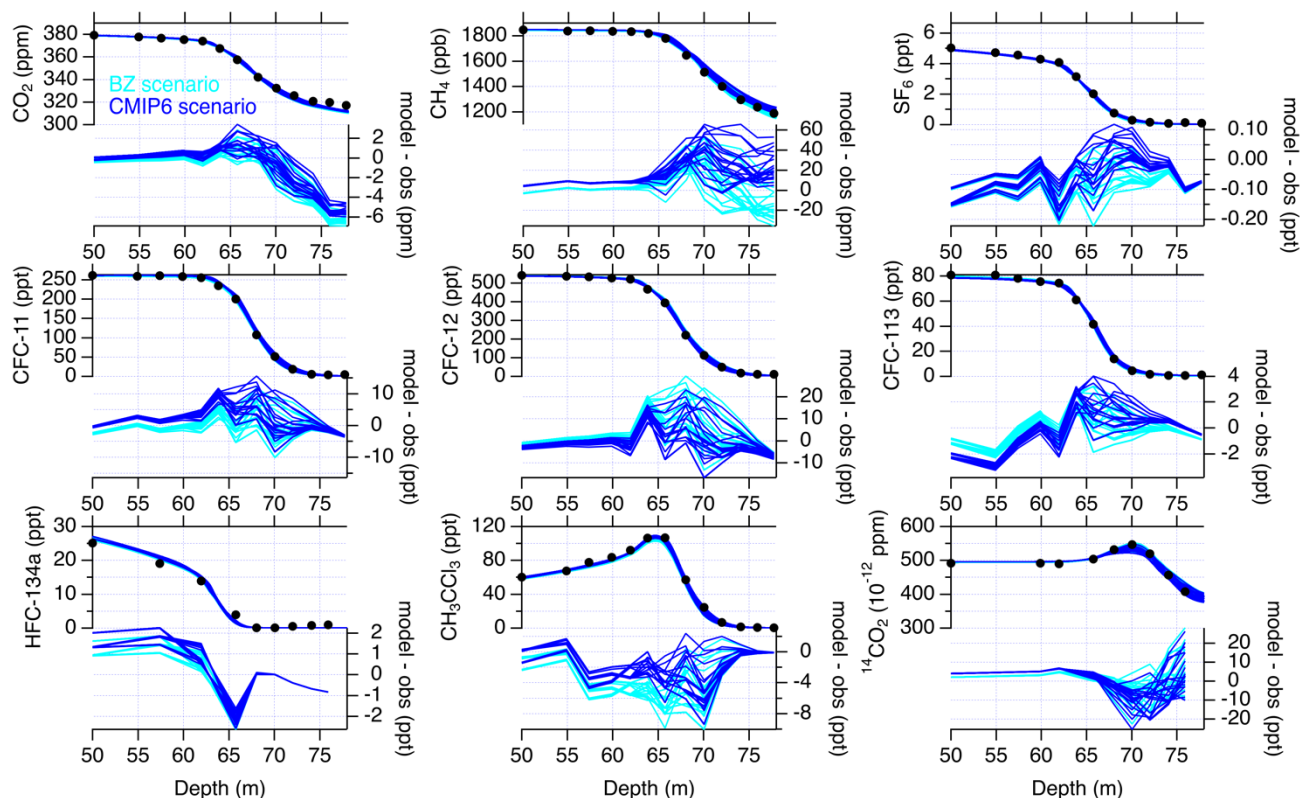
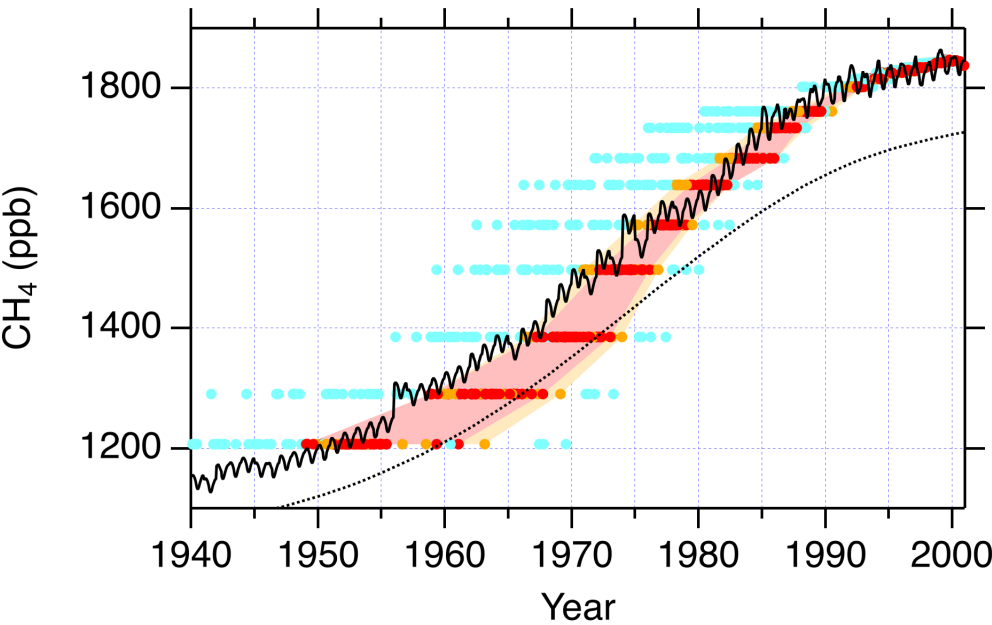


**Figure 9. Same as Figure 7, but for the NEEM firn. Only the simulation results with RMSD values of <1.0 are shown.**

## 4.2 Reconstruction by iterative dating

We explore the possibility of reconstructing the Arctic CH<sub>4</sub> mole fractions by the iterative dating method. This approach ~~sets~~ ~~the~~ ~~has a fixed~~ diffusivity profile ~~fixed~~ (assumed to be correct) and aims to find an acceptable atmospheric history to reproduce the firn-air depth profile. It is considered that the modified diffusivity profiles with the low RMSD values ~~for the six trace gases~~ are adequately evaluated by the trace gases except CH<sub>4</sub> and that the model-data mismatch in the CH<sub>4</sub> modeling is therefore attributable to uncertainty in the atmospheric CH<sub>4</sub> scenario. The historical atmospheric CH<sub>4</sub> ~~scenarios~~ variations obtained by the iterative dating method are presented in Figure 710 for the 100 modeling cases of the modified diffusivity. The different simulation cases are colored in the same manner as in the earlier figures according to the RMSD (Figures 4-3, 6 and 8). Note that the reconstruction cases colored in light blue are considered to be less likely, due to poorer reproduction of the depth profiles (Figures 56 and 68). The ~~model~~ NGRIP reconstruction results ~~in (red and orange, Figure 10a)~~ are in good agreement with the ~~initial atmospheric~~ BZ scenario by Buizert et al. (2012) after around 1980. For the earlier period, however, the upper bounds of the reconstructions ~~matches~~ match with the initial BZ scenario, and the overall range of acceptable histories

is below the ~~initial atmospheric CH<sub>4</sub>BZ~~ scenario (circles and shades in red and orange), suggesting). On the other hand, the  
450 ~~NEEM reconstruction results show that the CH<sub>4</sub> mole fractions may have been lower than the initial modeling range of~~  
~~acceptable histories are distributed closely around the original BZ scenario, or below it after around 1960, whereas the lower~~  
~~bound of the reconstruction aligns with the BZ scenario before that (Figure 10b).~~



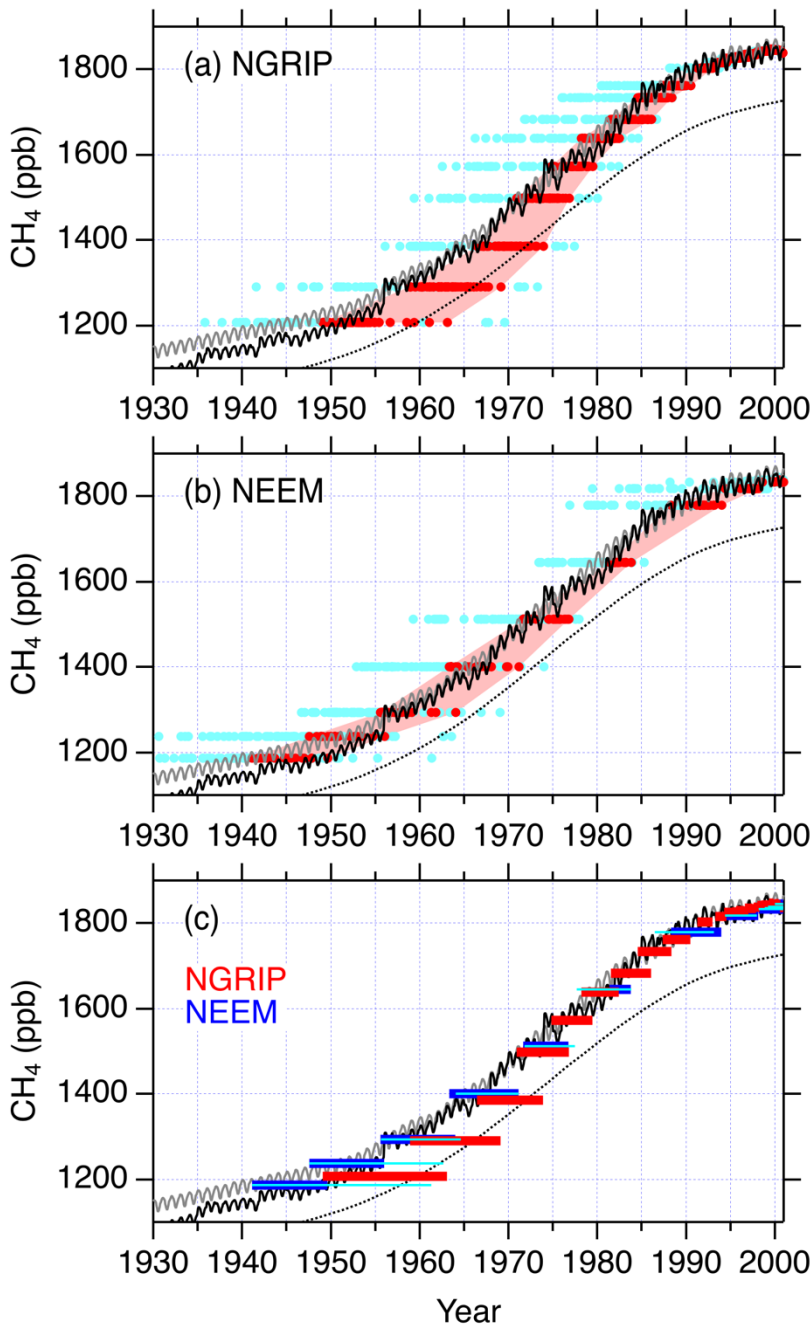


Figure 710: Results of reconstructions by the iterative dating method ~~from the NGRIP firn air (colored circles)~~ for the model cases with the 100 different diffusivity profiles (~~circles~~ colored in the same manner as in Figures 53, 6 and 6-8) ~~from the (a) NGRIP and (b) NEEM firn air, and (c) the ranges of reconstructions from both firn.~~ The ~~orange and~~ red shades indicate the range of CH<sub>4</sub> mole fraction trends reconstructed using the diffusivity profiles that better reproduce the ~~other six~~ trace gases except CH<sub>4</sub>. Black and grey solid line is the initial atmospheric CH<sub>4</sub> scenario (Buizert et al., 2012), scenarios of BZ and CMIP6, respectively, and black dotted line is the smoothed Antarctic CH<sub>4</sub> mole fraction (spline curve) from the Antarctic data shown in Figure 1. The thick

horizontal bars in red and blue in panel c correspond to red shades in panels a and b. The light blue thin bars in panel c indicate the range of the reconstructions for cases in which  $^{14}\text{CO}_2$  data are excluded for evaluations of the diffusivity profiles.

It should be stressed that the reconstructions for the time period before 1980 rely on ~~the~~  $\text{CH}_4$  data from the lowest ~~three~~ four or five depths of the NGRIP and NEEM firn air. The differences between the initial and corrected atmospheric  $\text{CH}_4$  scenario from ~~these~~ the three deepest data for the NGRIP firn are up to  $\sim 100$  ppb. As seen in Figure 710, such reduction in the Arctic atmospheric  $\text{CH}_4$  scenario over the period would result in alignment with the atmospheric  $\text{CH}_4$  trend in Antarctica inferred from the Law Dome and other datasets (black dotted line). It is again noted that all the reconstruction cases colored in ~~orange~~ and red used diffusivity profiles that yield relatively good model reproducibility with RMSD values of  $< 1.0$  ~~and 0.75~~, respectively. It is therefore seen that iterative dating-based reconstruction from the NGRIP firn data suggests decreased  $\text{CH}_4$  mole fraction from the 1950s to 1970s in any case, albeit with large uncertainty. It is however noted that, as shown in Figure 10c, this result is not fully compatible with that from the NEEM firn. In particular, the discrepancies between the reconstructions from both firn data diverge with time before 1970. When compared to these reconstructions, the BZ scenario (black line) tracks the overlapping ranges of both reconstructions, while the CMIP6 scenario passes above them before around 1955.

#### **4.3 Comparison to the NEEM profile**

~~To further evaluate consistency of the atmospheric  $\text{CH}_4$  scenario reconstructed from the NGRIP firn, we ran the model for the NEEM firn using the corrected atmospheric  $\text{CH}_4$  histories obtained from the iterative dating approach. The modeling results with the initial and modified atmospheric  $\text{CH}_4$  histories are shown in Figure 8. With the initial scenario (black line), the model-data difference was  $< 25$  ppb, with relatively large differences appearing in the LIZ ( $> 63$  m). However, when the atmospheric  $\text{CH}_4$  histories reconstructed from the NGRIP firn were employed, the reconstruction cases based on the improved reproducibility for the NGRIP firn (orange and red lines) resulted in larger model-data differences of  $> 50$  ppb in the LIZ.~~

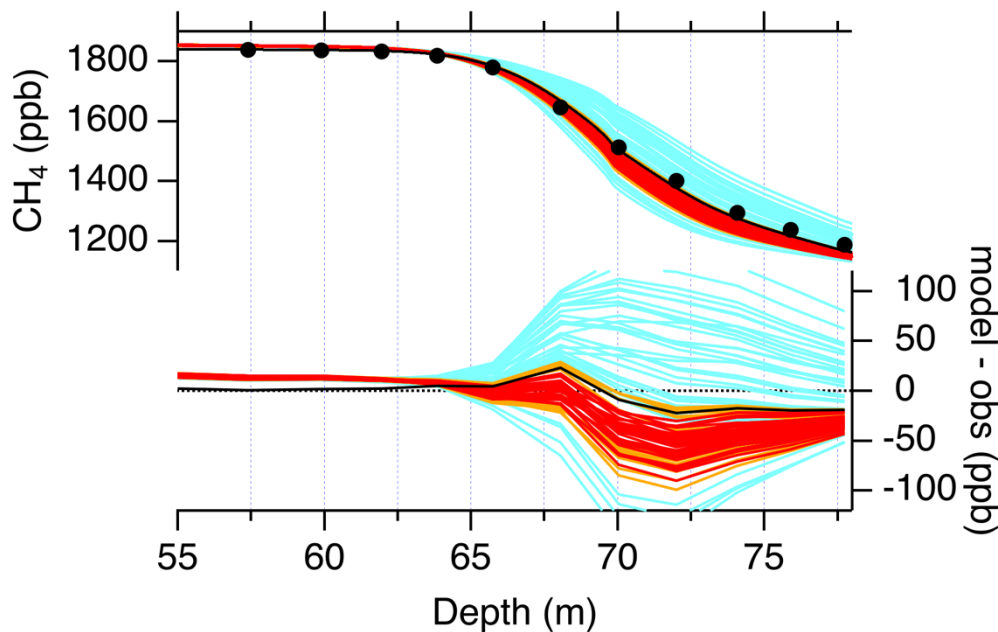


Figure 8: Depth profiles of CH<sub>4</sub> mole fraction in the NEEM firn at depths below 55 m. The measurements are shown by solid black circles. The modeling results with the atmospheric CH<sub>4</sub> scenario by Buizert et al. (2012) and with the CH<sub>4</sub> histories estimated from the NGRIP reconstruction are shown by black and colored lines, respectively (left axis). Corresponding model-data differences are also shown (right axis).

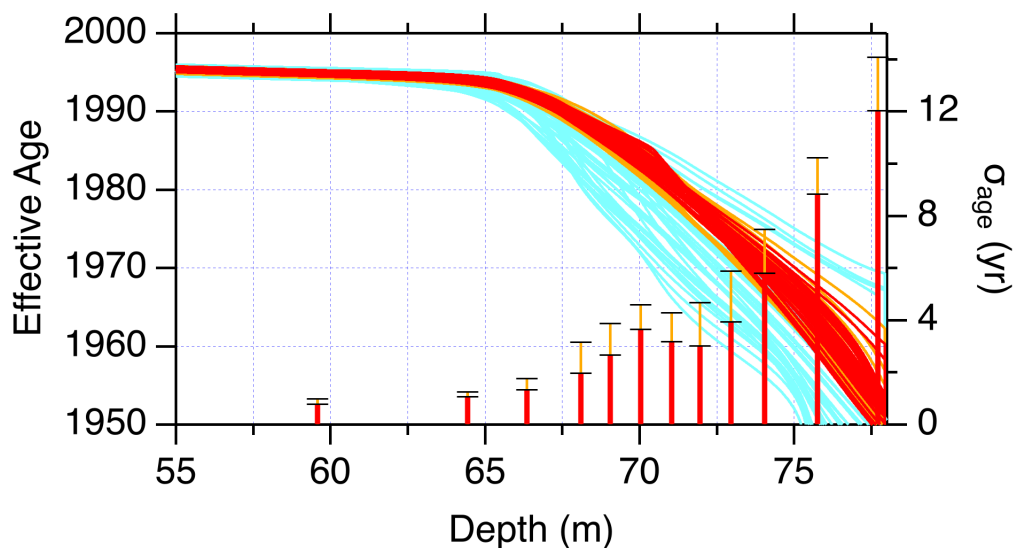
## 5 Discussion and conclusion

In section 4, we have shown that, with the two atmospheric scenarios prepared for the NEEM firn (BZ and CMIP6), depth profiles of CO<sub>2</sub>, SF<sub>6</sub>, CFC-11, CFC-12, CFC-113 and CH<sub>3</sub>CCl<sub>3</sub> in the NGRIP and NEEM firn are accurately reproduced with sufficient accuracy by using the range of modified diffusivity profiles (Figure 5 Figures 6, 7 and 9). This suggests that the atmospheric scenarios of these trace gases used in the modeling are consistent with the depth profiles observed at both firn sites in Greenland (NEEM and NGRIP). In contrast, the observed CH<sub>4</sub> profile in the NGRIP firn was not accurately reconciled using the two atmospheric scenario prepared for the NEEM firn scenarios and the diffusivity profiles that allow adequate reproducibility for the above six trace gases: (except CH<sub>4</sub>). This suggests either that the Arctic atmospheric scenarios scenarios of CH<sub>4</sub> is are uncertain or that the diffusivity profile of the NGRIP firn is underconstrained.

We explored the correction of the atmospheric scenario of CH<sub>4</sub> by the iterative dating approach. This method improves agreement to the observed CH<sub>4</sub> depth profile in the NGRIP firn, with an implicit assumption that the diffusivity profile in each case is correct. Although uncertainty due to the under-constrained diffusivity profile in the LIZ is large, this attempt for the NGRIP firn suggested that the CH<sub>4</sub> mole fractions over the period 1950–1980 could be decreased in comparison to the original BZ scenario prepared for the NEEM modeling (Figure 7). However, the follow-up modeling with the corrected atmospheric

CH<sub>4</sub> histories by the iterative dating based on the NGRIP data did not show improved reproducibility for the CH<sub>4</sub> profile at the NEEM site (Figure 8). It is therefore implied that neither the original CH<sub>4</sub> scenario by Buizert et al. (2012) nor the corrected CH<sub>4</sub> histories by this study, are well validated against the available two Greenland firn data sets (NGRIP and NEEM).<sup>10</sup> The decrease of up to 100 ppb from the ~~original~~BZ scenario over the period 1950–1980, as suggested by the iterative dating ~~in this study for the NGRIP firn~~, would make the CH<sub>4</sub> mole fraction as low as that in Antarctica (Figure 710). We point out that such a nearly-zero IPD of the CH<sub>4</sub> mole fraction is highly unlikely, given that a major fraction of both natural and anthropogenic CH<sub>4</sub> sources resides in the northern hemisphere in both preindustrial and industrial periods (Houweling et al., 2000; Ghosh et al., 2015; Saunois et al., 2020; Chandra et al., 2021). In contrast, the iterative dating reconstruction for the NEEM firn agrees with the BZ scenario. Although the spread of the reconstructions is large, particularly for the NGRIP firn, it was found that the BZ scenario passes within the ranges of the reconstructions from both firn data, but that the CMIP6 scenario is notably higher than the reconstructions for the period before 1960. This suggests that the BZ scenario is more consistent with the two sets of the Greenland firn data sets (NGRIP and NEEM) than the CMIP6 scenario for the mid 20th century when the two scenarios begin to diverge as time goes back.

It is important to note that the reconstructions for the period before 1980 from the NGRIP firn were heavily influenced by the ~~threefive~~ deepest data in the LIZ (> ~~7472~~ m). Figure 911a shows distributions of the effective age of CH<sub>4</sub> at depths below 55 m in the NGRIP firn, colored the same as in the earlier figures. In addition, the spread of the effective age ( $\sigma_{\text{age}}$ ) at each sampling depth is shown on the right axis. This figure shows that firn–air samples collected at the ~~threefive~~ lowest sampling depths at NGRIP have effective ages corresponding to the period from ~1950 to the ~~midlate~~ 1970s. In additionAt those depths, even the acceptable diffusivities yield the spread of the effective age of >5 years at those depths (red and orange (black vertical bars)). This shows that the reconstruction of the CH<sub>4</sub> mole fraction for the period is subject to much uncertainty in effective age. For the NEEM firn, the reconstructions before 1980 also rely on the five deepest data in the LIZ (Figure 11b). The  $\sigma_{\text{age}}$  values at those depths in the NEEM firn ranges from 5 to 8 years (thick vertical bars), comparable to those in the NGRIP firn. The Antarctic atmospheric CH<sub>4</sub> record (see Figures 1 and 710) indicates that the atmospheric increase rate of CH<sub>4</sub> was 10–15 ppb yr<sup>-1</sup> over the period. The 5-year uncertainty in the age estimate for the NGRIP firn–air samples could therefore be translated to an uncertainty of >50 ppb in the Arctic atmospheric CH<sub>4</sub> level. This is comparable to the IPD of CH<sub>4</sub> mole fraction during the 1950s to 1970s, which was assumed when Buizert et al. ~~(2012) prepared the Arctic atmospheric CH<sub>4</sub> scenario for the NEEM modeling~~(2012) prepared the BZ CH<sub>4</sub> scenario. It is also interesting to note that  $\sigma_{\text{age}}$  at the four deepest depths in the NEEM firn is almost constant, whereas it increases with depth in the NGRIP firn and exceeds 10 years at the two deepest depths. This indicates that effective age in the oldest firn-air layers can be estimated with better accuracy in the NEEM firn than in the NGRIP firn, thereby providing the reconstructions with smaller uncertainties. As  $\sigma_{\text{age}}$  was calculated from the simulation cases with acceptable ranges of diffusivity, its magnitude reflects how tightly the diffusivity profile is constrained at each firn site. In other words, our simulations infer that the diffusivity profile in the NEEM firn can be better constrained than the NGRIP firn.



545

550

Figure 9 In order to see the degree of constraint to the effective diffusivity from different trace gases, we calculated RMSD values for different combinations of the trace gases for the NEEM firn. The choice of the NEEM firn is due to the availability of a larger number of gas species. It was found that the  $^{14}\text{CO}_2$  data provide strong constraints for narrowing the acceptable range of diffusivity profiles in the LIZ. The evaluated RMSD with the  $^{14}\text{CO}_2$  data excluded and the historical  $\text{CH}_4$  reconstruction from the simulation cases with  $\text{RMSD} < 1.0$  is presented in Figure 10c (thin horizontal bars in light blue). The corresponding spread of the effective age is also shown in Figure 11b (thin vertical bars in black). These results show that, for the NEEM reconstruction, uncertainty of the effective age would be doubled at the two deepest depths if it were not for the  $^{14}\text{CO}_2$  data. It is also interesting that the range of the  $\text{CH}_4$  reconstruction without  $^{14}\text{CO}_2$  would deviate to the younger ages and would suggest a historical trend lower than the BZ scenario (Figure 10c). In turn, the  $\text{CH}_4$  trend reconstructed from the NGRIP firn might be different if  $^{14}\text{CO}_2$  measurement was available. The above contribution of the  $^{14}\text{CO}_2$  data for the NEEM firn implies that the NGRIP reconstruction could have been closer to the NEEM reconstruction. It is also noted that constraints from halocarbon species to the diffusivity profile are relatively weak as their mole fractions in the LIZ are decreased to close to zero.

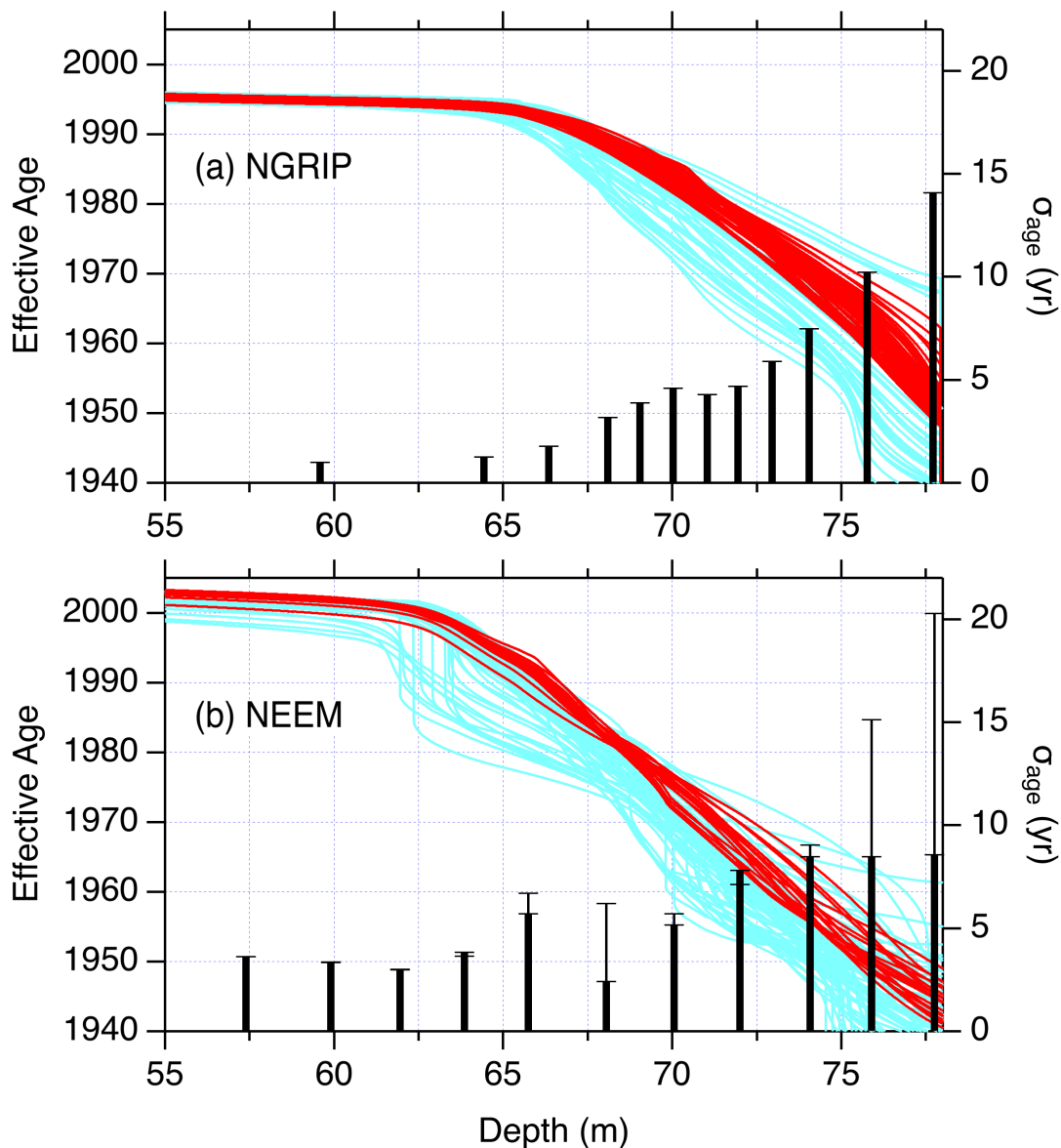


**Figure 11:** Depth profiles of effective age of CH<sub>4</sub> calculated after the iterative dating calculations for depths below 55 m at the (a) NGRIP and (b) NEEM firn sites (left axis). The solid lines represent cases for different diffusivity profiles and are colored in the same manner as in Figures 4-8, the earlier figures. Vertical orange and red bars in black indicate spread of the effective age (maximum minus minimum) at the individual sampling depths among the modeling cases in red. For the NEEM firn, the thin vertical bars correspond to the spread for simulation cases in which <sup>14</sup>CO<sub>2</sub> data are excluded for evaluations of the diffusivity profiles.

The IPD of the atmospheric CH<sub>4</sub> mole fraction is important for better understanding the evolution of the global CH<sub>4</sub> budget. Given that the Antarctic ice core and firn measurements have provided relatively reliable CH<sub>4</sub> records over the 20th century,



improved reconstructions from Greenland ice cores and firn air should better constrain the changes in the IPD. To sufficiently constrain the historical global CH<sub>4</sub> budget, the reconstruction for Greenland needs to be accurate within ~10 ppb, corresponding to ~30 Tg CH<sub>4</sub> yr<sup>-1</sup> global emission. Unfortunately, based on the firn CH<sub>4</sub> data from NGRIP and NEEM, this study demonstrated that consistent and accurate reconstruction of the Arctic CH<sub>4</sub> mole fraction is achievable only back to the mid 1970s, and that the uncertainty of reconstruction is still very large (around 50 ppb) for the 1950s to 1970s.

Previous studies have used CH<sub>4</sub> as one of tracers that constrain diffusivity profiles in firn (Witrant et al., 2012; Trudinger et al., 2013). These studies have shown that CH<sub>4</sub> effectively contributed to constraining diffusivity for deep layers i.e. LIZ in the NEEM firn. However, the use of CH<sub>4</sub> as ~~a strong~~ an effective constraint is valid only when its atmospheric scenario given as input to the models was assumed to be correct. Figures 56 and 68 show a larger spread in the model-data differences of CH<sub>4</sub> among the different diffusivity cases spread widely in the deepest layers of the LIZ of the NGRIP firn, in comparison to the other six gases. This fact highlights that subtle changes of the diffusivity profile in the LIZ have a large impact on simulating

CH<sub>4</sub>, and it indeed indicates that the species could serve as an effective diffusivity constraint, if its atmospheric scenario was correctly given with low uncertainty. ~~Although the currently proposed Arctic CH<sub>4</sub> history (Buizert et al., 2012) appears a useful choice in firn modeling at Greenland sites,~~ This study indicated that the two currently available Greenland firn data sets (NGRIP and NEEM) prefer the BZ CH<sub>4</sub> scenario (Buizert et al., 2012) over the CMIP6 scenario (Meinshausen et al., 2017). Furthermore, it should be again pointed out that the CMIP6 scenario suggests an almost constant IPD of ~130 ppb over the 20th century (Figure 2). Such constant IPD is unlikely, because CH<sub>4</sub> emissions are considered to have increased in the northern hemisphere for that period, which requires IPD to increase with time as discussed in the previous studies (Dlugokencky et al. 2003; Ghosh et al., 2015; Chandra et al., 2021). Accordingly, the BZ scenario appears a useful choice in firn modeling at Greenland sites, but it should be kept in mind that the use of CH<sub>4</sub> as a tuning tracer could lead to overfitting of the diffusivity profile.

Sapart et al. (2013) examined the reconstruction of stable carbon isotope ratio ( $\delta^{13}\text{C}$ ) of atmospheric CH<sub>4</sub> using firn–air measurements from both northern and southern hemispheres. They concluded that, with the available firn measurements and understanding of firn–air transport, it is difficult to reliably reconstruct the past trend of  $\delta^{13}\text{C}$  of CH<sub>4</sub> because of multiple reasons including uncertainty in the atmospheric CH<sub>4</sub> mole fraction scenario. Although there are many important and uncertain factors, the accurate reconstruction of the atmospheric CH<sub>4</sub> mole fraction is particularly important, because the trend in the mole fraction can lead to significant signal in the modeled  $\delta^{13}\text{C}$  profile in firn due to the difference in the molecular diffusion coefficient, even in the absence of a temporal trend in atmospheric  $\delta^{13}\text{C}$ . This study revealed a large uncertainty in the Arctic CH<sub>4</sub> mole fraction trend over the 20th century, which supports the conclusion of Sapart et al. (2013) on the difficulty of reconstruction of the  $\delta^{13}\text{C}$  of atmospheric CH<sub>4</sub> in the northern hemisphere. The NGRIP firn–air samples were also analyzed for  $\delta^{13}\text{C}$  and stable hydrogen isotope ratio ( $\delta\text{D}$ ) of CH<sub>4</sub> (Kawamura et al., 2021), but we regrettably report that reconstruction of  $\delta^{13}\text{C}$  of CH<sub>4</sub> ~~is difficult~~ has not been possible despite our best modeling efforts (not shown).

A possibility to improve the reproducibility of the depth profile of CH<sub>4</sub> in the NGRIP firn ~~may~~ could come from additional constraint to the diffusivity profile along with those currently made by the six trace gases (CO<sub>2</sub>, SF<sub>6</sub>, CFC-11, CFC-12, CFC-113 and CH<sub>3</sub>CCl<sub>3</sub>). ~~It could be performed by introducing additional effective tracers e.g.~~ In particular, it was indicated that

<sup>14</sup>CO<sub>2</sub>, ~~although such measurements cannot be foreseen for the~~ if available, would have strongly constrained the diffusivity profile and reduced uncertainty of the historical CH<sub>4</sub> trend reconstructed from the NGRIP ~~samples~~ firn. This study showed that, ~~with~~ the currently available firn data from Greenland (NGRIP and NEEM), ~~reliable~~ are in better agreement with the historical CH<sub>4</sub> scenario prepared for the NEEM firn modelling (Buizert et al., 2012), then that for the CMIP6 experiments (Meinshausen et al., 2017). Since the latter scenario relies on the NEEM-S1 ice core data (Rhodes et al., 2013), this study highlighted inconsistency between the ice core and two sets of firn data in Greenland. Given that reconstruction of the Arctic CH<sub>4</sub> mole fraction history ~~(independent of Antarctic records and assumed IPD) from the deepest firn layers~~ is possible back to the mid 1970s only. For the earlier period, consistent reconstruction with a small uncertainty of age estimate is currently difficult. ~~Future~~challenging (in terms of the diffusivity versus history problem as shown in this study), future sampling and measurements of ice cores at a high-accumulation site in Greenland (where age of air occluded can be determined accurately) may be the only way to reconstruct the atmospheric CH<sub>4</sub> trend over the 20th century.

### Data Availability

The composition data of the NGRIP firn-air samples are available on the Arctic Data archive System (ADS) of National Institute of Polar Research (<https://ads.nipr.ac.jp/dataset/A20210609-001>). The NEEM firn-air data are available in the supplementary file of Buizert et al. (2012). The CMIP6 historical scenarios of the various trace gases used in this study are available via <https://esgf-node.llnl.gov/search/input4mips/> as described in Meinshausen et al. (2017). Those of <sup>14</sup>CO<sub>2</sub> are available in the supplementary file of Graven et al. (2017). Our modeling data are available upon request ([umezawa.taku@nies.go.jp](mailto:umezawa.taku@nies.go.jp)).

### Author Contribution

TU, SS, KK and IO discussed on design of the study. KK, SA and TN conducted firn-air sampling at the NGRIP site. SS, KK, TU and TS analyzed the firn-air samples for trace gases. SJA set up the measurement system for the halocarbons. TU and SS made firn-air model simulations. TU analyzed the measurement/modeling data and prepared the manuscript with contributions from all co-authors.

### Completing interests

The authors declare that they have no conflict of interest.

## Acknowledgements

We thank Morimasa Takata at Nagaoka University of Technology for assisting the sample collection, and Jakob Schwander at University of Bern for collaboration at NGRIP. The NGRIP project was directed and organized by the Department of Geophysics at the Niels Bohr Institute for Astronomy, Physics and Geophysics, University of Copenhagen. It is supported by funding agencies in Denmark (SNF), Belgium (FNRS-CFB), France (IPEV and INSU/CNRS), Germany (AWI), Iceland (RannIs), Japan (MEXT), Sweden (SPRS), Switzerland (SNF) and the USA (NSF, Office of Polar Programs). We are grateful to the efforts for the measurement and modeling data from NOAA/ESRL/GML and the NEEM firn campaign, both of which are made freely available. This work was supported by JSPS/MEXT (Japan) KAKENHI Grants-in-Aid for Young Scientists B (17K18342 for TU), Grants-in-Aid for Scientific Research on Innovative Areas (17H06320 for KK) and the GRENE Arctic Climate Change Research Project (for SA). We thank the two anonymous referees for helpful comments to improve the manuscript.

## References

- Aoki, S., Nakazawa, T., Murayama, S., and Kawaguchi, S.: Measurements of atmospheric methane at the Japanese Antarctic Station. *Syowa. Tellus B*, 44, 273–281, <https://doi.org/10.1034/j.1600-0889.1992.t01-3-00005.x>, 1992.
- Blunier, T., Chappellaz, J. A., Schwander, J., Barnola, J.-M., Despert, T., Stauffer, B., and Raynaud D.: Atmospheric methane, record from a Greenland Ice Core over the last 1000 year, *Geophys. Res. Lett.*, 20(20), 2219–2222, <https://doi.org/10.1029/93GL02414>, 1993.
- Buizert, C., Martinerie, P., Petrenko, V. V., Severinghaus, J. P., Trudinger, C. M., Witrant, E., Rosen, J. L., Orsi, A. J., Rubino, M., Etheridge, D. M., Steele, L. P., Hogan, C., Laube, J. C., Sturges, W. T., Levchenko, V. A., Smith, A. M., Levin, I., Conway, T. J., Dlugokencky, E. J., Lang, P. M., Kawamura, K., Jenk, T. M., White, J. W. C., Sowers, T., Schwander, J., and Blunier, T.: Gas transport in firn: multiple-tracer characterisation and model intercomparison for NEEM, Northern Greenland, *Atmos. Chem. Phys.*, 12, 4259–4277, <https://doi.org/10.5194/acp-12-4259-2012>, 2012.
- Chandra, N., Patra, P. K., Bisht, J. S. H., Ito, A., Umezawa, T., Saigusa, N., Morimoto, S., Aoki, S., Janssens-Maenhout, G., Fujita, R., Takigawa, M., Watanabe, S., Saitoh, N., and Canadell, J. G.: Emissions from the oil and gas sectors, coal mining and ruminant farming drive methane growth over the past three decades, *J. Meteorol. Soci. Jpn.*, 99, <https://doi.org/10.2151/jmsj.2021-015>, 2021.
- Dlugokencky, E. J., Houweling, S., Bruhwiler, L., Masarie, K. A., Lang, P. M., Miller, J. B., and Tans P. P.: Atmospheric methane levels off: Temporary pause or a new steady-state?, *Geophys. Res. Lett.*, 30, 19, <https://doi.org/10.1029/2003GL018126>, 2003.
- Etheridge, D. M., Steel, L. O., Francey, R. J., and Langenfelds, R. L.: Atmospheric methane between 1000 A.D. and present: evidence of anthropogenic emissions and climatic variability, *J. Geophys. Res.*, 103, 15979–15993, <https://doi.org/10.1029/98JD00923>, 1998.

- 655 Francey, R. J., Manning, M. R., Allison, C. E., Coram, S. A., Etheridge, D. M., Langenfelds, R. L., Lowe, D. C., and Steele, L. P.: A history of  $\delta^{13}\text{C}$  in atmospheric  $\text{CH}_4$  from the Cape Grim Air Archive and Antarctic firn air, *J. Geophys. Res.*, 104(D19), 23631–23643, <https://doi.org/10.1029/1999JD900357>, 1999.
- Fujita, R., Morimoto, S., Umezawa, T., Ishijima, K., Patra, P. K., Worthy, D. E. J., Goto, D., Aoki, S., and Nakazawa, T.: Temporal variations of the mole fraction, carbon, and hydrogen isotope ratios of atmospheric methane in the Hudson Bay Lowlands, Canada, *J. Geophys. Res.: Atmos.*, 123, 4695–4711, <https://doi.org/10.1002/2017JD027972>, 2018.
- 660 Ghosh, A., Patra, P. K., Ishijima, K., Umezawa, T., Ito, A., Etheridge, D. M., Sugawara, S., Kawamura, K., Miller, J. B., Dlugokencky, E. J., Krummel, P. B., Fraser, P. J., Steele, L. P., Langenfelds, R. L., Trudinger, C. M., White, J. W. C., Vaughn, B., Saeki, T., Aoki, S., and Nakazawa, T.: Variations in global methane sources and sinks during 1910–2010, *Atmos. Chem. Phys.*, 15, 2595–2612, <https://doi.org/10.5194/acp-15-2595-2015>, 2015.
- 665 Graven, H., Allison, C. E., Etheridge, D. M., Hammer, S., Keeling, R. F., Levin, I., Meijer, H. A. J., Rubino, M., Tans, P. P., Trudinger, C. M., Vaughn, B. H., and White, J. W. C.: Compiled records of carbon isotopes in atmospheric  $\text{CO}_2$  for historical simulations in CMIP6, *Geosci. Model Dev.*, 10, 4405–4417, <https://doi.org/10.5194/gmd-10-4405-2017>, 2017.
- Houweling, S., Dentener, F., and Lelieveld, J.: Simulation of preindustrial atmospheric methane to constrain the global source strength of natural wetlands, *J. Geophys. Res.*, 105(D13), 17243–17255, <https://doi.org/10.1029/2000JD900193>, 2000.
- 670 Ishijima, K., Sugawara, S., Kawamura, K., Hashida, G., Morimoto, S., Murayama, S., Aoki, S., and Nakazawa, T.: Temporal variations of the atmospheric nitrous oxide concentration and its  $\delta^{15}\text{N}$  and  $\delta^{18}\text{O}$  for the latter half of the 20th century reconstructed from firn air analyses, *J. Geophys. Res.*, 112, D03305, <https://doi.org/10.1029/2006JD007208>, 2007.
- Kawamura, K., Severinghaus, J. P., Ishidoya, S., Sugawara, S., Hashida, G., Motoyama, H., Fujii, Y., Aoki, S., and Nakazawa, T.: Convective mixing of air in firn at four polar sites, *Earth Planet. Sci. Lett.*, 244, 3–4, 672–682, <https://doi.org/10.1016/j.epsl.2006.02.017>, 2006.
- 675 Kawamura, K., Umezawa, T., Sugawara, S., Ishidoya, S., Ishijima, K., Saito, T., Oyabu, I., Murayama, S., Morimoto, S., Aoki, S., and Nakazawa T.: Composition of firn air at the North Greenland Ice Core Project (NGRIP) site, *Polar Data J.*, ~~in~~ [press](https://doi.org/10.20575/00000030)5, 89–98, [http://doi.org/10.20575/00000030](https://doi.org/10.20575/00000030).
- Landais, A., Barnola, J. M., Kawamura, K., Caillon, N., Delmotte, M., Van Ommen, T., Dreyfus, G., Jouzel, J., Masson-Delmotte, V., Minster, B., Freitag, J., Leuenberger, M., Schwander, J., Huber, C., Etheridge, D., Morgan, V.: Firn-air  $\delta^{15}\text{N}$  in modern polar sites and glacial-interglacial ice: a model-data mismatch during glacial periods in Antarctica? *Quaternary Sci. Rev.*, 25, 49–62, <https://doi.org/10.1016/j.quascirev.2005.06.007>, 2006.
- 680 MacFarling Meure, C., Etheridge, D., Trudinger, C., Steele, P., Langenfelds, R., van Ommen, T., Smith, A., and Elkins, J.: Law Dome  $\text{CO}_2$ ,  $\text{CH}_4$  and  $\text{N}_2\text{O}$  ice core records extended to 2000 years BP, *Geophys. Res. Lett.*, 33, L14810, <https://doi.org/10.1029/2006GL026152>, 2006.
- 685 Martinerie, P., Nourtier-Mazauric, E., Barnola, J.-M., Sturges, W. T., Worton, D. R., Atlas, E., Gohar, L. K., Shine, K. P., and Brasseur, G. P.: Long-lived halocarbon trends and budgets from atmospheric chemistry modelling constrained with measurements in polar firn, *Atmos. Chem. Phys.*, 9, 3911–3934, <https://doi.org/10.5194/acp-9-3911-2009>, 2009.

- Meinshausen, M., Vogel, E., Nauels, A., Lorbacher, K., Meinshausen, N., Etheridge, D. M., Fraser, P. J., Montzka, S. A.,  
690 Rayner, P. J., Trudinger, C. M., Krummel, P. B., Beyerle, U., Canadell, J. G., Daniel, J. S., Enting, I. G., Law, R. M.,  
Lunder, C. R., O'Doherty, S., Prinn, R. G., Reimann, S., Rubino, M., Velders, G. J. M., Vollmer, M. K., Wang, R. H. J.,  
and Weiss, R.: Historical greenhouse gas concentrations for climate modelling (CMIP6), *Geosci. Model Dev.*, 10, 2057–  
2116, <https://doi.org/10.5194/gmd-10-2057-2017>, 2017.
- Monteil, G., Houweling, S., Dlugokenky, E. J., Maenhout, G., Vaughn, B. H., White, J. W. C., and Röckmann, T.: Interpreting  
695 methane variations in the past two decades using measurements of CH<sub>4</sub> mixing ratio and isotopic composition, *Atmos.*  
*Chem. Phys.*, 11, 9141–9153, <https://doi.org/10.5194/acp-11-9141-2011>, 2011.
- Nakazawa, T., Machida, T., Tanaka, M., Fujii, Y., Aoki, S., and Watanabe, O.: Differences of the atmospheric CH<sub>4</sub>  
concentration between the Arctic and Antarctic regions in pre-industrial/pre-agricultural era, *Geophys. Res. Lett.*, 20943–  
20946, <https://doi.org/10.1029/93GL00776>, 1993.
- 700 Oyabu, I., Kawamura, K., Kitamura, K., Dallmayr, R., Kitamura, A., Sawada, C., Severinghaus, J. P., Beaudette, R., Orsi, A.,  
Sugawara, S., Ishidaoya, S., Dahl-Jensen, D., Goto-Azuma, K., Aoki, S., Nakazawa, T.: New technique for high-precision,  
simultaneous measurements of CH<sub>4</sub>, N<sub>2</sub>O and CO<sub>2</sub> concentrations; isotopic and elemental ratios of N<sub>2</sub>, O<sub>2</sub> and Ar; and  
total air content in ice cores by wet extraction, *Atmos. Meas. Tech.*, 13(12), 6703–6731. [http://doi.org/10.5194/amt-13-](http://doi.org/10.5194/amt-13-6703-2020)  
6703-2020, 2020.
- 705 Rhodes, R. H., Faïn, X., Stowasser, C., Blunier, T., Chappellaz, J., McConnell, J. R., Romanini, D., Mitchell, L. E., Brook, E.  
J.: Continuous methane measurements from a late Holocene Greenland ice core: Atmospheric and in-situ signals, *Earth*  
*Planet. Sci. Lett.*, 368, 9–19, <https://doi.org/10.1016/j.epsl.2013.02.034>, 2013.
- Rice, A. L., Butenhoff, C. L., Teama, D. G., Röger, F. H., Khalil, M. A. K., and Rasmussen, R. A.: Atmospheric methane  
isotopic record favors fossil sources flat in 1980s and 1990s with recent increase, *Proc. Natl. Acad. Sci.*, 113(39), 10791–  
710 10796, <https://doi.org/10.1073/pnas.1522923113>, 2016.
- Rigby, M., Montzka, S. A., Prinn, R. G., White, J. W. C., Young, D., O'Doherty, S., Lunt, M. F., Ganesan, A. L., Manning,  
A. J., Simmonds, P. G., Salameh, P. K., Harth, C. M., Mühle, J., Weiss, R. F., Fraser, P. J., Steele, L. P., Krummel, P. B.,  
McCulloch, A., and Park, S.: Role of atmospheric oxidation in recent methane growth, *Proc. Natl. Acad. Sci.*, 114(21),  
5373–5377. <https://doi.org/10.1073/pnas.1616426114>, 2017.
- 715 Rommelaere, V., Arnaud, L., and Barnola, J.-M.: Reconstructing recent atmospheric trace gas concentrations from polar firm  
and bubbly ice data by inverse methods, *J. Geophys. Res.*, 102(D25), 30069–30083, <https://doi.org/10.1029/97JD02653>,  
1997.
- Saito, T., Yokouchi, Y., Aoki, S., Nakazawa, T., Fujii, Y., and Watanabe, O.: A method for determination of methyl chloride  
concentration in air trapped in ice cores, *Chemosphere*, 63(7), 1209–1213,  
720 <https://doi.org/10.1016/j.chemosphere.2005.08.075>, 2006.
- Sapart, C. J., Monteil, G., Prokopiou, M., van de Wal, R. S. W., Kaplan, J. O., Sperlich, P., Krumhardt, K. M., van der Veen,  
C., Houweling, S., Krol, M. C., Blunier, T., Sowers, T., Martinerie, P., Witrant, E., Dahl-Jensen, D., and Röckmann, T.:

Natural and anthropogenic variations in methane sources during the past 2 millennia, *Nature*, 490, 85–88, <https://doi.org/10.1038/nature11461>, 2012.

- 725 Sapart, C. J., Martinerie, P., Witrant, E., Chappellaz, J., van de Wal, R. S. W., Sperlich, P., van der Veen, C., Bernard, S.,  
Sturges, W. T., Blunier, T., Schwander, J., Etheridge, D., and Röckmann, T.: Can the carbon isotopic composition of  
methane be reconstructed from multi-site firn air measurements? *Atmos. Chem. Phys.*, 13, 6993–7005,  
<https://doi.org/10.5194/acp-13-6993-2013>, 2013.
- Saunois, M., Staver, A. R., Poulter, B., Bousquet, P., Canadell, J. G., Jackson, R. B., Raymond, P. A., Dlugokencky, E. J.,  
730 Houweling, S., Patra, P. K., Ciais, P., Arora, V. K., Bastviken, D., Bergamaschi, P., Blake, D. R., Brailsford, G., Bruhwiler,  
L., Carlson, K. M., Carrol, M., Castaldi, S., Chandra, N., Crevoisier, C., Crill, P. M., Covey, K., Curry, C. L., Etiope, G.,  
Frankenberg, C., Gedney, N., Hegglin, M. I., Höglund-Isaksson, L., Hugelius, G., Ishizawa, M., Ito, A., Janssens-  
Maenhout, G., Jensen, K. M., Joos, F., Kleinen, T., Krummel, P. B., Langenfelds, R. L., Laruelle, G. G., Liu, L., Machida,  
T., Maksyutov, S., McDonald, K. C., McNorton, J., Miller, P. A., Melton, J. R., Morino, I., Müller, J., Murguía-Flores,  
735 F., Naik, V., Niwa, Y., Noce, S., O'Doherty, S., Parker, R. J., Peng, C., Peng, S., Peters, G. P., Prigent, C., Prinn, R.,  
Ramonet, M., Regnier, P., Riley, W. J., Rosentreter, J. A., Segers, A., Simpson, I. J., Shi, H., Smith, S. J., Steele, L. P.,  
Thornton, B. F., Tian, H., Tohjima, Y., Tubiello, F. N., Tsuruta, A., Viovy, N., Voulgarakis, A., Weber, T. S., van Weele,  
M., van der Werf, G. R., Weiss, R. F., Worthy, D., Wunch, D., Yin, Y., Yoshida, Y., Zhang, W., Zhang, Z., Zhao, Y.,  
Zheng, B., Zhu, Q., Zhu, Q., and Zhuang, Q.: The Global Methane Budget 2000–2017, *Earth Syst. Sci. Data*, 12, 1561–  
740 1623, <https://doi.org/10.5194/essd-12-1561-2020>, 2020.
- Schwander, J.: The transformation of snow to ice and the occlusion of gases. In: *The Environmental Record in Glaciers and  
Ice Sheets* (eds. H. Oeschger and C. C. Langway), John Wiley & Sons, Berlin 53–67, 1989.
- Schwander, J., Barnola, J.-M., Andrié, C., Leuenberger, M., Ludin, A., Raynaud, D., and Stauffer, B.: The age of the air in the  
firn and the ice at Summit, Greenland, *J. Geophys. Res.*, 98(D2), 2831–2838, <https://doi.org/10.1029/92JD02383>, 1993.
- 745 Severinghaus, J. P., Albert, M. R., Courville, Z. R., Fahnestock, M. A., Kawamura, K., Montzka, S. A., Mühle, J., Scambos,  
T. A., Shields, E., Shuman, C. A., Suwa, M., Tans, P., and Weiss, R. F.: Deep air convection in the firn at a zero-  
accumulation site, central Antarctica, *Earth Planet. Sci. Lett.*, 293, 359–367, <https://doi.org/10.1016/j.epsl.2010.03.003>,  
2010.
- Sowers, T., Bender, M., Raynaud, D., and Korotkevich, Y. S.:  $\delta^{15}\text{N}$  of  $\text{N}_2$  in air trapped in polar ice: A tracer of gas transport  
750 in the firn and a possible constraint on ice age-gas age differences, *J. Geophys. Res.*, 97(D14), 15683–15697,  
<https://doi.org/10.1029/92JD01297>, 1992.
- Stern, D. I., and Kaufmann, R. K.: Estimates of global anthropogenic methane emissions 1860–1993, *Chemosphere*, 33, 1,  
159–176, [https://doi.org/10.1016/0045-6535\(96\)00157-9](https://doi.org/10.1016/0045-6535(96)00157-9), 1996.
- Sturrock, G. A., Etheridge, D. M., Trudinger, C. M., Fraser, P. J., and Smith, A. M.: Atmospheric histories of halocarbons  
755 from analysis of Antarctic firn air: Major Montreal Protocol species, *J. Geophys. Res.-Atmos.*, 107, 4765,  
<https://doi.org/10.1029/2002JD002548>, 2002.

- Sugawara, S., Kawamura, K., Aoki, S., Nakazawa, T., and Hashida, G.: Reconstruction of past variations of  $\delta^{13}\text{C}$  in atmospheric  $\text{CO}_2$  from its vertical distribution observed in the firn at Dome Fuji, Antarctica, *Tellus, Ser. B*, 55, 159–169, <https://doi.org/10.1034/j.1600-0889.2003.00023.x>, 2003,
- 760 Sugawara, S., Ishidoya, S., Aoki, S., Morimoto, S., Nakazawa, T., Toyoda, S., Inai, Y., Hasebe, F., Ikeda, C., Honda, H., Goto, D., and Putri, F. A.: Age and gravitational separation of the stratospheric air over Indonesia, *Atmos. Chem. Phys.*, 18, 1819–1833, <https://doi.org/10.5194/acp-18-1819-2018>, 2018.
- Trudinger, C. M., Enting, I. G., Etheridge, D. M., Francey, R. J., Levchenko, V. A., Steele, L. P., Raynaud, D. and Arnaud, L.: Modeling air movement and bubble trapping in firn, *J. Geophys. Res.* 102, 6747–6763, <https://doi.org/10.1029/96JD03382>, 1997.
- 765 Trudinger, C. M., Etheridge, D. M., Rayner, P. J., Enting, I. G., Sturrock, G. A., and Langenfelds, R. L.: Reconstructing atmospheric histories from measurements of air composition in firn, *J. Geophys. Res.*, 107(D24), 4780, <https://doi.org/10.1029/2002JD002545>, 2002.
- Trudinger, C. M., Enting, I. G., Rayner, P. J., Etheridge, D. M., Buizert, C., Rubino, M., Krummel, P. B., and Blunier, T.: How well do different tracers constrain the firn diffusivity profile? *Atmos. Chem. Phys.*, 13, 1485–1510, <https://doi.org/10.5194/acp-13-1485-2013>, 2013.
- 770 Umezawa, T., Goto, D., Aoki, S., Ishijima, K., Patra, P. K., Sugawara, S., Morimoto, S., and Nakazawa, T.: Variations of tropospheric methane over Japan during 1988–2010, *Tellus B*, 66, 23837, <http://dx.doi.org/10.3402/tellusb.v66.23837>, 2014.
- 775 van Aardenne, J. A., Dentener, F. J., Olivier, J. G. J., Goldewijk, C. G. M. K., and Lelieveld, J.: A  $1^\circ \times 1^\circ$  resolution data set of historical anthropogenic trace gas emissions for the period 1890–1990, *Global Biogeochem. Cycles*, 15(4), 909–928, <https://doi.org/10.1029/2000GB001265>, 2001.
- Witrant, E., Martinerie, P., Hogan, C., Laube, J. C., Kawamura, K., Capron, E., Montzka, S. A., Dlugokencky, E. J., Etheridge, D., Blunier, T., and Sturges, W. T.: A new multi-gas constrained model of trace gas non-homogeneous transport in firn: evaluation and behaviour at eleven polar sites, *Atmos. Chem. Phys.*, 12, 11465–11483, <https://doi.org/10.5194/acp-12-11465-2012>, 2012.
- 780